Claudiomar Rodrigues Franco

Evaluation of a turn-off photoluminescent probe based on graphene quantum dots for the determination of Hg^{2+} in water samples using flow injection analysis.

Dissertação de Mestrado

Dissertation presented to the Programa de Pós-graduação em Química of PUC-Rio in partial fulfillment of the requirements for the degree of Mestre em Química.

Advisor: Prof. Ricardo Queiroz Aucélio

Co-Advisor: Dr. Luis Maqueira Espinosa

Rio de Janeiro
June 2019

Claudiomar Rodrigues Franco

Evaluation of a turn-off photoluminescent probe based on graphene quantum dots for the determination of Hg^{2+} in water samples using flow injection analysis.

Dissertation presented to the Programa de Pós-graduação em Química of PUC-Rio in partial fulfillment of the requirements for the degree of Mestre em Química. Approved by the undersigned Examination Committee.

Prof. Ricardo Queiroz Aucélio
Advisor
Departamento de Química - PUC-Rio

Dr. Luis Maqueira Espinosa
Co-advisor
Departamento de Química - PUC-Rio

Profª. Andrea Rosane da Silva
CEFET/RJ

Prof. José Marcus de Oliveira Godoy
Departamento de Química - PUC-Rio

Prof. Jones Limberger
Departamento de Química - PUC-Rio

Rio de Janeiro, June 28th 2019.

Claudiomar Rodrigues Franco

Master's degree candidate in the Chemistry Graduate Program at Pontifícia Universidade Católica do Rio de Janeiro (PUC-Rio). He obtained a Licentiate degree in Chemistry, concluded in 2010, from the Instituto Federal Fluminense – Campos. He also holds an Associate's degree as a chemical technician, concluded in 2012. He has experience in the oil and gas industry, working for Baker Hughes as a Field Specialist from 2013 to 2016. He is currently working as a Laboratory Analyst at Expro do Brasil within the Fluid Analysis Center (FAC).

Acknowledgment

Firstly, I give thanks to God for giving me protection and strength to cope with all my struggles.

My special and heartily thanks to my advisor, Professor Ricardo Aucélio, for his constructivist teaching which is based on the belief that students learn best when they gain knowledge through exploration and active learning. He is a great role model who has encouraged and directed me throughout this journey. I am especially indebted to my co-advisor, Dr. Luis Maqueira, who has shown me, by his example, what a good scientist (and person) should be.

I give deep thanks to all the Professors and the Faculty of the Department of Chemistry and each of the members of my Dissertation Committee who has provided me extensive personal and professional guidance and taught me a great deal about both scientific research and life in general.

I am grateful to all of those with whom I have had the pleasure to work during these years in the laboratory (LEEA), especially Dra. Joseany Almeida, whose kindness is immeasurable.

To my beloved friend Pastor Rafael Antunes, founder of the orphanage I grew up since I was 8 years old and his honorable wife, aunt Rosimar Antunes who have shown me not to become a man of success, but rather a man of value. I also thank Mairy Cardoso who has been supportive of my career goals and all CEB faculties for the educational support.

I thank all whom in one way or another contributed in the completion of this dissertation.

May the Almighty God richly bless all of you.

Abstract

Franco, Claudiomar Rodrigues; Aucélio, Ricardo Queiroz (advisor); Espinosa, Luis Maqueira (Co-advisor). **Evaluation of a turn-off photoluminescent probe based on graphene quantum dots for the determination of Hg^{2+} in water samples using flow injection analysis.** Rio de Janeiro, 2019. 90p. Dissertação de Mestrado - Departamento de Química, Pontifícia Universidade Católica do Rio de Janeiro.

A photoluminescent turn-off probe was evaluated for the detection of Hg^{2+} based on graphene quantum dots (GQDs). Different photoluminescent carbon nanoparticles were prepared using the bottom-up approach, with citric acid and with citric acid mixed with some sulfur compound (thiourea, thioacetamide or glutathione). Dispersions of these GQDs were compared in terms of photophysical behavoior in the presence of Hg^{2+}. It was observed that the nanoparticles prepared with citric acid and thiourea (GQDs-TU) presented a better linear photoluminescent suppression (analytical response) in the presence of Hg^{2+}. Experimental conditions were adjusted to improve analytical response and to obtain analytical figures of merit. A study to evaluate potential interferences in the presence of other heavy metal ions and alkaline and alkaline-earth ions, commonly present in natural water samples. The normalized analytical curve (L_0/L *versus* Hg^{2+} concentration) was linear ($R^2 = 0.998$) up to 0.20 µmol L^{-1}. The limit of quantification (LOQ) was 10 µg L^{-1} and the limit of detection (LOD) was 3 µg L^{-1} for the batch assay. In addition, the proposed strategy for indirect determination of Hg^{2+} was applied in a flow injection analysis system (FIA). After optimization of the assay, linear range covered a range up to 900 µg L^{-1} ($R^2 = 0.999$) with LOD of 24 µg L^{-1} and LOQ of 80 µg L^{-1}. The recovery in the fortified water sample was 99.4%.

Keywords

Graphene quantum dots; photoluminescence; functionalized GQDs; mercury; flow injection analysis.

Resumo

Franco, Claudiomar Rodrigues; Aucélio, Ricardo Queiroz; Espinosa, Luis Maqueira. **Avaliação de uma sonda fotoluminescente do tipo turn-off baseado em pontos quânticos de grafeno para determinação de Hg^{2+} em amostra de água usando análise por injeção de fluxo.** Rio de Janeiro, 2019. 90p. Dissertação de Mestrado - Departamento de Química, Pontifícia Universidade Católica do Rio de Janeiro.

Uma sonda fotoluminescente do tipo "turn-off" foi avaliada para a detecção de Hg^{2+} usando pontos quânticos de grafeno (GQDs). Diferentes nanopartículas de carbono fotoluminescentes foram preparadas usando a abordagem bottom-up, usando ácido cítrico ou ácido cítrico misturado com algum composto contendo enxofre (tioureia, tioacetamida ou glutationa). Dispersões desses GQDs foram comparadas em termos de comportamento fotofísico na presença de Hg^{2+}. Observou-se que as nanopartículas preparadas com ácido cítrico e tioureia (GQDs-TU) apresentaram melhor perfil de supressão fotoluminescente (resposta analítica) na presença de Hg^{2+}. As condições experimentais foram ajustadas para o melhor perfil de resposta e para obter os parâmetros analíticos de mérito. Um estudo para avaliar possíveis interferências na presença de outros íons de metais pesados além de íons alcalinos e alcalino-terrosos, comumente presentes em amostras de água natural. A curva analítica normalizada (concentração L_0/L versus Hg^{2+}) foi linear ($R^2 = 0,998$) até 0,20 µmol L^{-1}. O limite de quantificação (LOQ) foi de 10 µg L^{-1} e o limite de detecção (LOD) foi de 3 µg L^{-1} para o ensaio em batelada. Além disso, a estratégia proposta para a determinação indireta de Hg^{2+} foi adaptada para um sistema de análise por injeção em fluxo (FIA). Após a otimização do ensaio, com a faixa linear cobrindo o intervalo até 900 µgL^{-1} ($R^2 = 0,999$), os valores de LOD e LOQ foram 24 µg L^{-1} e 80 µg L^{-1}, respectivamente. A recuperação na amostra simulada de água fortificada foi de 99,4%$\pm$1,2.

Palavras-chave

Pontos quânticos de grafeno; fotoluminescência; GQDs funcionalizados; mercúrio; análise por injeção em fluxo.

Table of contents

List of figures

List of tables

List of abbreviations

afGQD	Amino-functionalized gqds
ATP	Adenosine triphosphate
AuNP	Gold nanoparticles
CA	Citric acid
CDs	Carbon dots
CQDs	Carbon quantum dots
CV	Cyclic voltammogram
CV-AAS	Cold vapor atomic absorption spectrometry
DFT	Density functional theory
EGTA	Ethylene glycol-bis(B-aminoethylether)-N,N,N',N'-tetracetic acid
EIS	Electrochemical impedance spectroscopy
FIA	Flow injection analysis
FRET	Fluorescence resonance energy transfer
gGQDs	Greenish-yellow fluorescent gqds
GNRs	Graphene nanoribbons
GO	Graphene oxide
GQDs	Graphene quantum dots
GQDs-PEG	Gqds surface-passivated by polyethylene glycol
GSH	Glutathione
GSs	Graphene sheets
HOMO	Highest occupied molecular orbital
ICP-MS	Inductively coupled plasma-mass spectrometry
LOD	Limit of detection
LUMO	Lowest unoccupied molecular orbital
NSET	Surface energy transfer
ORR	Oxygen reduction reaction
PEG	Polyethylene glycol
PL	Photoluminescence
QDs	Quantum dots
QY	Quantum yield
SRM	Standard reference material
TA	Thioacetamide
TBAP	Tetrabutylammonium perchlorate
TGFRET	Time-gated fluorescence resonance energy transfer
TU	Thiourea

"The monotony of a quiet life stimulates the creative mind."
Albert Einstein

1
Introduction

1.1
Contextualization of work

Since the Minamata bay tragedy, in the 1950´s, it has been recognized the multiple pathways of mercury contamination, through air, water, food and even though pharmaceuticals and cosmetic products, and the serious impact posed by this element, in a myriad of forms, persisting in the environment and accumulating in organisms of the chain food. Amongst the forms of mercury, the organic forms are the most toxic, as they, owing to its liposolubility, passes the blood brain barrier. The damage has vast implications with mamals at the top of food chain, getting the worst impact due to biomagnification [1]. However, even inorganic mercury species such as mercury (II) are highly toxic being extremely harmful pollutants in aquatic ecosystems. Exposure to mercury might cause kidney and respiratory failures and neurological damage [2,3]. The contamination of drinking water by Hg^{2+} is still a commonly occurring incident, therefore it is important to find relatively cheap and easy ways to monitor the presence of Hg^{2+} above desired threshold levels in aqueous systems [4].

Mercury, especially Hg^{2+}, is amongst the species most targeted in terms of the development of analytical methods. Despite that, scientific literature continues to propose new analytical approaches involving improved detection, speciation, sample preparation and pre-concentration. In fact, in terms of limits of detection, background limited determinations (at low ng L^{-1} levels or sub pg absolute levels) have been comfortably achieved by using inductively coupled plasma spectrometry (ICP-MS) [5] and atomic fluorescence spectrometry (AFS) [6], also enabling speciation when coupled respectively with high-performance liquid chromatography (HPLC) [7] and gas chromatography (GC) [8]. However, the best compromise between sensitivity and selectivity has been achieved by cold vapor atomic

absorption detection (CV-AAS) [9]. Other scientific fronts involves pre-concentration strategies that enables the use of techniques less sensitive towards mercury such as molecular spectrophotometry [6] and off-line speciation aiming the simplification, in terms of complexity and cost, of the required analytical apparatuses.

Even with several available analytical methods and strategies towards mercury, new studies are frequently found in recent literature aiming to develop different electrochemical sensors [10–12] and photoluminescent sensors, in this case using, for instance, lanthanide complexes [13–15], covalent organic frameworks [16,17] and inorganic quantum dots [18–20]. The driving force behind the development of these different sensors is to enable affordable ways to selectively detect mercury (generally Hg^{2+}) enabling the indication of the presence of this pollutant above a determined concentration level, often dictated by the type of sample and the limit of quantification of the sensor. The general performance of these sensors in terms of degradation of response and limit of quantification and interferences allows for developing improved sensing devices and methods.

The development of eco-friendly optical sensing methods for simple and sensitive detection of mercury is highly desirable and thus stimulated. In recent years, the use of gold nanoparticles, semiconductor inorganic quantum dots (QDs) [21]–[24], fluorescent dyes [25], biomaterials [4, 21, 25] as sensors have been often proposed. Compared to other sensing strategies, the ones based upon luminescence from QDs show high effectiveness in terms of high sensitivity, resonable selectivity and simplicity in probing [27]. The QDs are nanometric size semiconductor materials (zero dimension materials as all their dimensions are measured within the nanoscale) that present special properties due to the quantum confinement effect, in which valence and conductance bands become quantized and the gap between the highest valence energy level and the lowest conductance energy level depends upon nanoparticle size [28,29]. Depending upon the production process, QDs can be easily stabilized in aqueous solutions, forming a nanoparticle dispersion with very large surface area to interact with other substances in solution [30].

In recent years, carbon dots (CDs) have attracted interest because they can produce photoluminescence as intense as semiconductor inorganic QDs but being nanostructures composed mainly by carbon, which is very interesting in terms of low toxicity and thus compatible to biomedical applications [31]. Carbon nanoparticles prepared by hydro-exfoliation tend to produce sheets of carbon with small dimensions (<100 nm), isolated or in a multilayered arrangement, regarded as graphene quantum dots (GQDs). They tend to produce intense photoluminescence as result of quantum confinement and can produce highly stable aqueous dispersions in water, being prone to interact with solutes, producing changes in measured photoluminescence, mainly in terms of intensity and/or spectral position [32]. Furthermore, the edge functionalization of GQDs, obtained under production conditions, may improve photoluminescence and provide some selectivity in interaction with the target chemical species [33,34].

The novelty of this work is to study different GQDs, produced using a mixture of citric acid and chemical modifiers containing sulfur (thiourea, thioacetamide, and glutathione), aiming to produce a good sensor for Hg^{2+}. After stablishing the GQDs with the highest potential for the task, experimental conditions to the disperse GQDs were adjusted aiming to promote better analytical response (probe conditions), in this case through a quenching effect ('turn-off' mechanism) induced by Hg^{2+}. Literature also lacks information on the use of GQDs in terms of comparison of analytical determinations using stationary regime (batch analysis) with GQDs dispersed in water inside a cuvette with flow analysis regime. The automation of the method using a flow injection analysis (FIA) system was used to minimize the influence from the kinetics that affects signal response (improving precision) and to significantly reduce labor intensity, typical of batch analysis [35]. The influence of alkaline and alkaline earth ions were evaluated as they are the major components found in mineral waters.

1.2
Dissertation structure

This dissertation is structured in 6 chapters. In Chapter 1, a brief contextualization of the work and their objectives are presented. In Chapter 2 presents the theoretical framework aiming to provide the basic understanding of theories and concepts that are relevant to the topic of the research. Brief information about the targeted analyte is presented, followed by a brief revision of the analytical methods for its determination in water samples. In addition, this section briefly summarizes about QDs and GQDs covering their production, physical and chemical proprieties and some reported analytical methods using graphene quantum dots and quantum dots for mercury sensing. Finally, a description of the flow injection analysis is briefly made pointing out its operating process and listing the advantages of using an automatic method of analysis.

Chapter 3 contains detailed information about the employed instrumentation, materials and reagents also presenting the procedures employed to prepare solutions and samples and the procedures concerning the analytical methods.

The results and discussions of the study carried out for the indirect determination of mercury by using GQDs are presented in Chapter 4. This section includes i) characterization of GQDs and the GQDs-Hg^{2+} interaction kinetic study; ii) the study to adjust conditions in order to maximize photoluminescent responses of GQDs-TU towards Hg^{2+}; iii) a study to investigate quenching mechanism; iv) an evaluation of the selectivity of GQDs towards Hg^{2+} and a study to minimize interferences found in mineral waters; v) the method validation and the quantitative determination of Hg^{2+} in water samples by standard addition method; and vii) the application of method in a flow injection system.

Finally, in Chapter 5 and Chapter 6 are devoted to the conclusions and directions for future works, respectively.

1.3
Objectives

1.3.1
General objective

The goal of this work is to evaluate the feasibility of using different graphene quantum dots as probes for the indirect determination of mercury in water samples also evaluating the use of flow injection analysis for this task.

1.3.2
Specific objectives

- ✓ Produce different GQDs, characterizing the most responsive to Hg^{2+} using different optical and morphologic analyses.
- ✓ Evaluate photoluminescent response (sensitivity and kinetics) of these different GQDs towards the analyte of interest;
- ✓ Study of the assay conditions (pH, temperature, buffering conditions) that provide adequate photoluminescent responses for the determination of inorganic mercury;
- ✓ Study of interaction between the most responsive GQDs and Hg^{2+};
- ✓ Study of the interference imposed by alkaline and alkaline earth ions.
- ✓ Adjust and compare analysis regimes (batch assay and flow injection analysis).
- ✓ Apply the method in a controlled sample.

2
Theoretical framework

2.1
Mercury

The contamination of the environment by mercury has been of crucial concern throughout the world for decades. Mercury, as the only liquid metal at normal conditions, has many unique properties that make it useful in various industrial applications. At the same time, mercury compounds are highly toxic causing kidney injury, central nervous system disorders, intellectual deterioration, and eventualy death [36].

Mercury is ubiquitous in the environment, approximately 10,000 tons originates from degassing of earth's crust, to this amount approximately 20,000 tons/year is added by anthropogenic activity [1]. Mercury emissions from the coal smoke is the main source of anthropogenic discharge and mercury pollution in atmosphere [37]. Another important source of mercury pollution is the artisanal and small-scale gold mining, which accounts for more than a third of global emissions [38]. Mercury emission in air eventually goes into rivers, lakes and oceans after travelling long distances together with wind. In aquatic environments, inorganic mercury is microbiologically transformed into lipophilic organic compound, mainly methylmercury. This transformation makes mercury more prone to biomagnification in food chains. Consequently, populations with traditionally high dietary intake of food originating from fresh or marine environment have highest dietary exposure to mercury.

Because of the danger posed by mercury and mercury compounds to the society and to the environment, the "Minamata Convention on Mercury" was ratified, in 2017. That is a global aggrement that include "ban on new mercury mines, the phase-out of existing ones, the phase out and phase down of mercury use in a number of products and processes, control measures on emissions to air and on releases to land and water, and the regulation of the informal sector of artisanal and small-scale gold mining"

[39]. The Convention also addresses "interim storage of mercury and its disposal once it becomes waste, sites contaminated by mercury as well as health issues" [39].

There have been numerous studies dedicated to the study of mercury toxicity. F. Zharir *et al* (2005) have shortlisted some of the effects due to low dose mercury exposure to humans (Table 1).

Table 1 - Effect of low dose mercury toxicity on various organ systems[1].

Nervous system Adults	Memory loss, including Alzheimer like dementia, deficit in attention, hypoesthesia, ataxia, dysarthrea, subclinical finger tremor impairment of hearing and vision, sensory disturbances, increased fatigue.
Children/infants	Deficit in language (late talking) and memory deficit in attention, Autism.
Motor system Adults	Disruption of fine motor function; decreased muscular strength, increased tiredness.
Children/infants	Late walking Increases.
Renal system	Increases plasma creatinine level
Cardiovascular system Immune	Alters normal cardiovascular homoeostasis.
Immune system	Decreases overall immunity of the body, exacerbates lupus like autoimmunity, multiple sclerosis, autoimmune thyroiditis or atopic eczema.
Reproductive system	Decreases rate of fertility in both males and females, birth of abnormal offsprings.

In fact, the use of mercury in industrial processes increased significantly following the industrial revolution of the 19th century. According to the WHO (World Health Organization) levels of mercury in rainwater are in the range 5–100 ng L^{-1}, but mean levels as low as 1 ng L^{-1} have been reported [40]. Naturally occurring levels of mercury in groundwater and surface water are less than 0.5 µg L^{-1}, although local mineral deposits may produce higher levels in groundwater [41]. Inorganic mercury is the most common form that is present in drinking water but is not considered to be very harmful to human health, in terms of the levels found, but kidney damage may result from exposure to inorganic mercury through other sources. In 1974, the EPA (Environmental Protection Agency) established the Safe Drinking Water Act that set specific guidelines on contaminants

that are commonly found in drinking water. However, it was not until 1992 that mercury, in particular, became regulated. Both the Maximum Contaminant Level Goal and the Maximum Contaminant Level were set at 2 µg L^{-1} since current technology allows public water suppliers to detect and remove mercury levels that low [42].

2.2
Analytical methods for mercury determination in water samples

As one of the most toxic metals, mercury pollution has attracted much attention in environmental and toxicological domains thus making mercury and mercury based compounds probably the most targeted analyte in the scientific literature concerning the effort in developing analytical methods for determination/speciation and propose sample preparation/preservation as well as analyte pre-concentration. Despite that, developing effective methods for mercury is in high demand even for water samples. Passariello *et al.* (1996) used inductively coupled plasma mass spectrometry (ICP-MS) for the direct determination of ultratrace mercury (detection limit of 0.001 µg L^{-1}) in potable water, due to the choice of interference-free isotopes by the mass spectrometer detector [5]. By using with HPLC in tandem, ICP-MS becomes a tool able to detect, at the same detection power, different species of mercury [43]. Similar lower levels of mercury has been achieved by cold vapor (CV) atomic fluorescence spectrometry (AFS) using a mercury dedicated system [44]. When coupled to gas chromatography (GC) speciation capability can be achieved after derivatization, generaly using a propylation derivative agent [45].

The cold vapor atomic absorption spectrometry (AAS) has been a compromise between sensitivity and cost effectiveness, due the relatively simplicity of instrumentation, enabling some possibility for speciation using, for instance photo-oxidation of the organic mercury (indirectly measured as total mercury). J. Murphy *et al* (1996) developed an accurate and sensitive method for determining mercury in environmental and biological samples using a microwave digestion and using flow injection analysis (FIA) with on-line CV-AAS system for mercuy detection. By coupling FIA and CV-AAS, a

considerable increasing in analytical frequency was achieved compared to the conventional CV-AAS analysis. The method offers a limit of detection (LOD) of 0.2 ng g^{-1} and precision of less than 10% (evaluated using standard reference materials) [9]. Manová *et al.* (2012) determined mercury in water samples by graphite furnace atomic absorption spectrometry after the preconcentration of Hg (II) on a gold working electrode in a flow system coupled on-line to the AAS instrument. The porous electrode was made of glassy carbon particles coated with gold. Tap, river, and wastewater samples were analyzed using this method. The method enabled them to determine Hg in the concentration range of 0.05 to 60 μg L^{-1}. Detection limit and precision were found to be 53 ng L^{-1} and 5.9%, respectively [46].

Niazi *et al.* (2009) investigated a cloud point extraction process, using the nonionic surfactant Triton X-114, for extracting mercury from aqueous solutions prior to its spectrophotometric determination. Linearity was obeyed in the range of 5.0–80.0 ng mL^{-1} of Hg^{2+}. The method was applied to the determination of mercury in water samples and the LOD of the method was 0.83 ng mL^{-1} of Hg^{2+} [47].

Other electrochemical methods have also been proposed such as the one reported by Lin *et al.* (2011) consisting of an unlabeled immobilized DNA-based sensor to detect Hg^{2+} through the use of the difference in charge-transfer resistance before and after DNA interactions with Hg^{2+}, which were monitored by electrochemical impedance spectroscopy (EIS). The change in signal was sufficient to enable LOD of 0.1 nmol L^{-1} (0.02 μg L^{-1}) for Hg^{2+}. Moreover, the sensor maintained high selectivity over other nonspecific metal ions [26].

Moreover, in recent years, many reports dedicated to alternative sensing devices for mercury have been published. The development of mercury sensors based on metal nanoparticles [21–24], fluorescent dyes [45,46], among other, offers an alternative route to overcome the limitation of traditional mercury detection methods due to their simplicity. The analytical characteristics including the linear range and detection limit of some familiar fluorimetric methods for Hg(II) detection with organic fluorescent dyes and QDs as fluorescence probe are summarized in Table 2.

Table 2 - Comparison of the linear range and detection limit of several methods for detection for Hg (II) with organic fluorescent dyes and inorganic QDs as fluorescence probe.

Sensor	Linear range (10⁻⁷ mol L⁻¹)	LOD (10⁻⁹ mol L⁻¹)	Ref
TGA @ AuNPs–RB sensor	0.01-0.35	0.60	[49]
AuNPs-TGA+Rh6G sensor	0.005–0.355	0.06	[48]
MAA-capped InP QDs	25.00–398.00	997.00	[51]
L-cysteine-capped CdSe	0.00–20.00	6.00	[52]

In terms of fluorescent dyes, Chen *et al.* (2007) developed a gold-nanoparticles (AuNPs)–Rhodamine 6G (Rh6G) based fluorescent sensor for detecting Hg(II) in aqueous solution. The Rh6G dye was strongly fluorescent in bulk solution; however, quenching occurred in the presence of AuNPs, as result of fluorescence resonance energy transfer. With the addition of Hg(II), signal gradually recovered due to fact that Rh6G molecules departed from the surface of the AuNPs. They applied the method in real environmental water samples with satisfactory results (recovery between 96 and 102%) [48]. Zheng *et al.* (2009) developed a sensitive "switch-on" method for the determination of Hg(II) in waters using Rhodamine B (RB) capped AuNPs as a fluorescence sensor. The monodispersed and "naked" AuNPs were modified with thioglycolic acid (TGA) and the fluorescence from RB was quenched completely by the AuNPs surface, with negative charge, mainly as a result of fluorescence resonance energy transfer. Under the optimum conditions, the restoration fluorescence intensity is proportional to the concentration of Hg(II). The method was applied in environmental water samples and the results of recovery for four samples (98 to 104%) were satisfactory with a good agreement with the results obtained by atomic absorption spectroscopy (AAS) [49].

It is well known that semiconductor quantum dots (QDs) are attractive luminescent labels due to their high quantum efficiency, photostability, and size-tunable optical properties [23]. Unfortunately, these QDs usually contain toxic elements such as Cd, As and Pb that pose environmental concern even considering the very low concentrations of

QDs used in assays. An example of the use of QDs containing toxic element (Cd in this case) is the work reported by Chen *et al.* (2006) using mono-dispersed water-soluble CdSe nanoclusters functionalized with L-cysteine. Under optimized conditions, a good linear relationship was found between the logarithm of fluorescence intensity ratio of system and concentration of mercury ions. The recovery in river water sample were 96-98% [52]. An alternative to Cd based QDs is the use of non-toxic indium phosphide (InP) that also emits in the visible region of the spectrum. Following this strategy, Zhu *et al.* (2005) synthesized water-compatible InP nanocrystals capped with mercaptoacetic acid (MAA). The nanocrystals fluorescence (750/826 nm) was significantly enhanced in the presence of Hg^{2+} ions. Under the optimum conditions, the signal intensity was proportional to the concentration of Hg^{2+}[51].

2.3
Nanoparticles - Quantum dots

Nanomaterials are materials whose sizes of the constituent particles are in the range of nanometers, at least in one dimension. Nanomaterials have gained significant importance in the late 20th century, inducing an entire area of knowledge, now recognized as "Nanoscience and Nanotechnology" [53]. Nanoscience and nanotechnology involve the investigation and manipulation of matter on nanometer length scales (typically defined as 1-100 nm) and has led to the discovery of new phenomena and resulted in new technologies and applications, increasing, therefore, investiments from both governments and industries around the world [54].

An important class of nanomaterials is semiconductor nanocrystals or quantum dots (QDs). A quantum dot is a 0D material as it has all three dimensions confined to the 1- to 10 nm-length scale [55]. Because they are in nanometric scale, the semiconductor nanoparticles have strong quantum confinement (the smaller the nanocrystal, the greater the confinement of electrons), which is a fundamental factor that justifies the photoluminescence characteristics of these QDs. Quantum confinement is

responsible for the quantization of the valence and the conductance bands of semiconductors, which presents as degenerated levels when semiconductor present itself in microscale. Ekimov, using a glassy matrix, and Brus, from colloidal dispersions, discovered the QDs in the early 1980s. The most common QDs are those consisting of the groups II-VI, III-V and IV-VI of the periodic table, being the most common group II-VI atoms, for instance, CdS, CdSe, CdTe [53-54].

In terms of the optical characteristics, QDs have a broad absorption band, size tuneable spectral emission, higher photostability, and emission lifetime ranging between several hundreds of picosecond and tenths of nanosecond. In addition, selective detection has been achieved for colloidal QDs by means of chemical functionalization. In fact, the characteristics of the QDs may vary depending on the presence of agents that coat the surface of the QDs, for instance, organic ligants [58]. It is also important to mention that physical and chemical properties of II-VI QDs generally depend on size. For example, their optical absorption spectra generally exhibit a peak at the threshold, which is assigned to the creation of excitons.

Excitons is a *quasi*-particle formed by an electron-hole pair. It is formed when an electron is promoted from one quantized level of the valence band to an equaly quantizied level from the conductance band, leaving a vacancy behind. The position and the shape of this peak are strongly dependent on the nanocrystal sizes, which are inhomogeneously distributed considering a population of QDs [59]. In a nanocrystal of small size, typically for a radius lower than the effective Bohr radius of the bulk excitation, the excitation has a larger kinetic energy because of the strong confinement [60]. As the size of a QDs decreases, the band gap increases, resulting in emission at shorter wavelengths. This quantum confinement effect is analogous to the quantum mechanical model "particle in a box," in which the energy of the particle increases as the size of the box decreases [61]. Taking a drastic case as an example, CdSe QDs having relatively small size (2 nm) absorb and emit light in the visible region, but when core-diameter reaches the range of 7-8 nm, it absorb and emit light in the deep-red and IR regions, respectively (Figure 1).
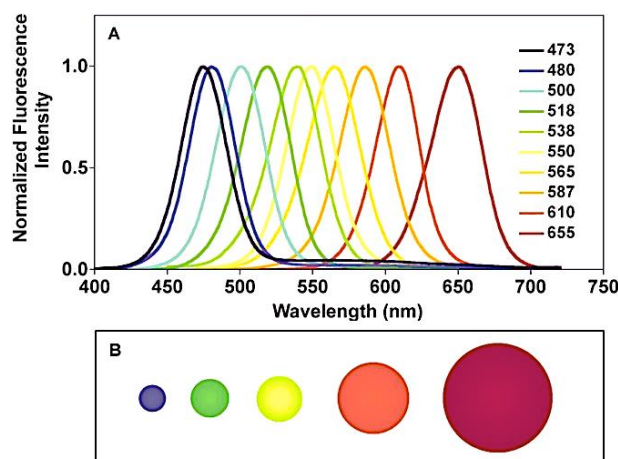
Figure 1 - Size-tunable fluorescence spectra of CdSe quantum dots (A), and illustration of the relative particle sizes (B). From left to right, the particle diameters are 2.1 nm, 2.5 nm, 2.9 nm, 4.7 nm, and 7.5 nm [61].

When dispersed in water, QDs may interact with solutes with consequent changes in photoluminescence characteristics (intensity, lifetime and spectral position). Selective interaction has been achieved by means of chemical modifications of the surface of QDs, for instance, some organic ligants [58]. Other efforts have been made to modifify surface of QDs with enzymes, antigens and even strains of DNA in order to lead to high selective interaction with species that affect QDs optical properties. As the magnitude of changes in optical properties is dependent upon the concentration of the interacting species, a quantitative model can be established and the QDs dispersion can be used as analytical luminescent sensors. In this matter, although other types of fluorophore such as fluorescent dyes have found valuable applications in differents areas (e.g. biology, technology, analytical chemistry), QDs seems to be providing more robust properties overcoming the limitations of organic dyes (such as photostability and solubility in water). It should be noted, however, that there are obstacles for the use of some semiconductor QDs in some *in vivo* applications because of the presence of toxic elements [62]. In addition, the same characteristics that make nanoparticles interesting in terms of technological applications may also be undesirable when they are released into the environment. The small size of the nanoparticles facilitates diffusion and transport in the atmosphere, in water, and in soils, while making them

difficult to remove by usual filtration techniques. It may also facilitate the entry and accumulation of nanoparticles into living cells [63].

2.4
Graphene quantum dots

In recent years, luminescent carbon dots (CDs) have attracted growing interest due to their optical properties, close alike of those of semiconductor QDs, and because their very simple structures (made basicaly of carbon). Therefore, they are becoming an attractive alternative in respect to nanomaterial-based applications, especially very promising for biomedical applications [31].

Graphene is a one-atom thick planar structure of carbon atoms arranged in a honeycomb crystal lattice [64]. As a two-dimensional (2D) single-atom carbon sheet, graphene has ignited tremendous research interest due to its large surface area, high intrinsic carrier mobility, strong mechanical strength, and superior flexibility. While the application of 2D graphene sheets (GSs) is limited by their nature of easy aggregation and poor dispersion in common solvents, the etching of graphene into one-dimensional (1D) stripes, known as graphene nanoribbons (GNRs), mitigated these problems and demonstrated the intriguing properties of confined transport gaps and quantum dots behavior associated with the geometry of these nanostructures of carbon. In the past few years, there has been an ongoing enthusiasm to further convert graphene to 0D graphene quantum dots (GQDs) and study their characteristics associated with quantum confinement and edge effects. These dots are usually biocompatible, strongly luminescent and well dispersed in various solvents, showing potential for integration into devices of bioimaging, photovoltaic and light emitting applications [65]. In comparison with conventional two-dimensional (2D) graphene, these 0D graphene quantum dots (GQDs) usualy manifest themselves as clusters stacked from several layers of graphene with nanometer diameter. They oftern contain some oxygen-rich functional groups, such as hydroxy, carboxyl, epoxy groups on their edges [66].

Compared to inorganic semiconductor QDs, the carbon based QDs seem to be less toxic as precursors are compounds such citric acid and ascorbic acid. GQDs in water produce highly stable dispersions and present stable optical properties, even when in solid phase and in contact to the air. GQDs are isolated nanosheets of graphene (flakes) with small dimensions (<100 nm) that produce intense photoluminescence as result of quantum confinement [32]. Furthermore, these nanoparticles may present easy surface and edge functionalization that may improve photoluminescence and provide some selectivity in the interaction with the target chemical species [33, 34], which makes them promising for photoluminescent probing.

2.4.1
Production of GQDs

Many methods for production of GQDs have been reported such as nanolithography technique [67], electrochemical scissoring [68], ultrasonic shearing [69], hydrothermal and solvothermal cutting of graphene sheets [62,63], nanotomy assisted exfoliation [72], precursor pyrolysis [73], stepwise organic synthesis [65], etc.

These approaches can be generally classified into two main groups: top-down and bottom-up methods. Depending on the experimental conditions employed, the properties and structure of the produced nanoparticles can be controlled. Routes for the synthesis of nanoparticles may, in principle, allow the control the particle size, particle geometry, doping ratio by different elements, and degree of particle agglomeration. These particle parameters give the synthesized nanomaterial new physical and chemical properties for different applications [74]. The top-down approaches refer to the cutting of graphene sheets into GQDs, the method consists of chemical ablation, electrochemical oxidation, and oxygen plasma treatment, where GQDs are formed or ''broken off'' from larger graphene sheets. Bottom-up methods involve the synthesis of graphene moieties containing a certain number of conjugated carbon atoms, the

approaches consist, for example, of the cage-opening of fullerene, or solution chemistry methods during which the GQDs are formed from molecular precursors [66]. A general scheme of these processes can be seen in Figure 2.
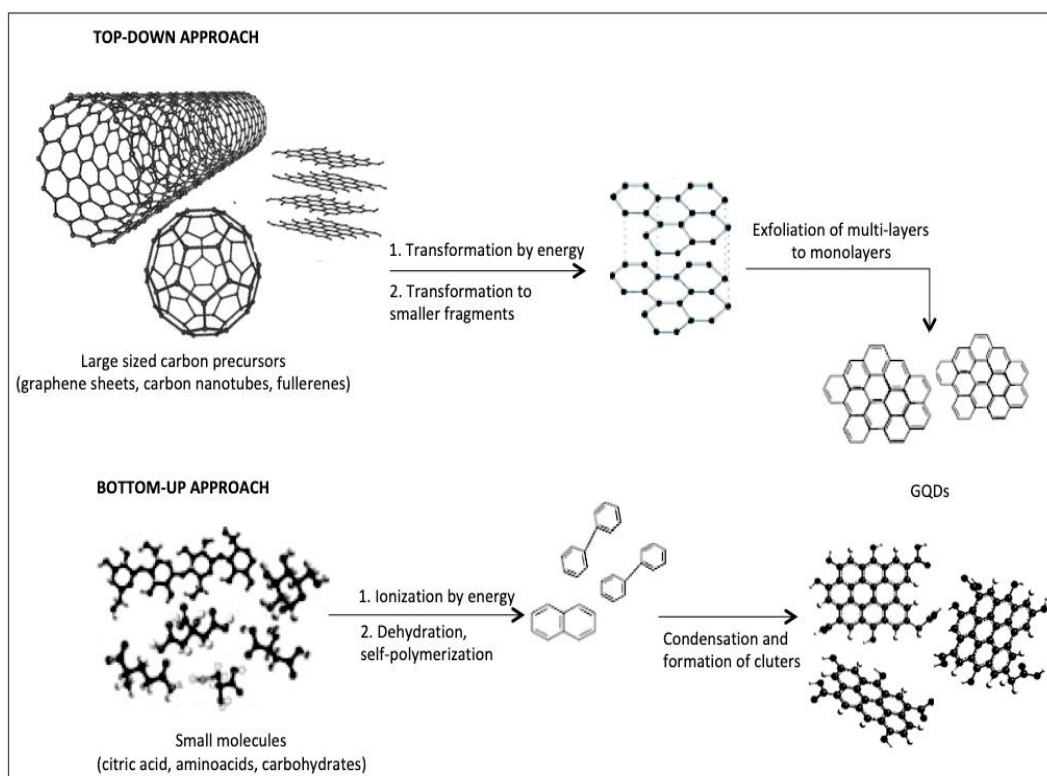
Figure 2 - Schematic diagram of top-down and bottom-up aproches for production of the GQDs. Adapted from J. Wang *et al.* (2015). [75]

The Table 3 shows a list of these strategies that provide capability to tune the properties of GQDs for various specific applications.

Table 3 – A brief summary of the typical synthetic strategies for GQDs (adapted from Z. Zhang *et al* (2012)) [65].

Synthetic strategies	Subclassification	Size of GQDs (nm)
Cutting approaches	Nanolithography technique	30 – 250
	Hydrothermal cutting of GSs	1.5 – 13
	Solvothermal cutting of GSs	5.3 (in average)
	Electrochemical scissoring of GSs	3 – 60
	Chemical exfoliation	1 – 18
	Nanotomy assisted exfoliation	10 – 50, according to the demand
	Ultrasonic shearing of GSs	3 – 5
Chemical synthesis	Stepwise organic synthesis of GQDs	~5
	Precursor pyrolysis	1.65 – 21 (depending on reaction time)

GQDs: graphene quantum dots; GSs: graphene sheets.

The hydro-exfoliation of melted organic material is a bottom-up approach that is characterized by its simplicity and efficiency. By carbonizing some specific organic precursors by a thermal treatment usually allows some control over the morphology and the size distribution of the products. The GQDs can be prepared by directly pyrolyzing a proper precursor (tuning the incomplete carbonization degree) such as citric acid or ascorbic acids and even mixtures of organic compounds then dispersing the melted material into a solvent system usualy aqueous. For instance, by melting citric acid and exfoliating in alkaline aqueous solutions. Dong *et al* (2015) obtained GQDs of about 15 nm in width and from 0.5 to 2.0 nm in thickness [76]. A complete carbonization leads to graphene oxide (GO) when the funcionalizations is supposed to occur within the carbon net, breaking the graphene net continuity (Figure 3).
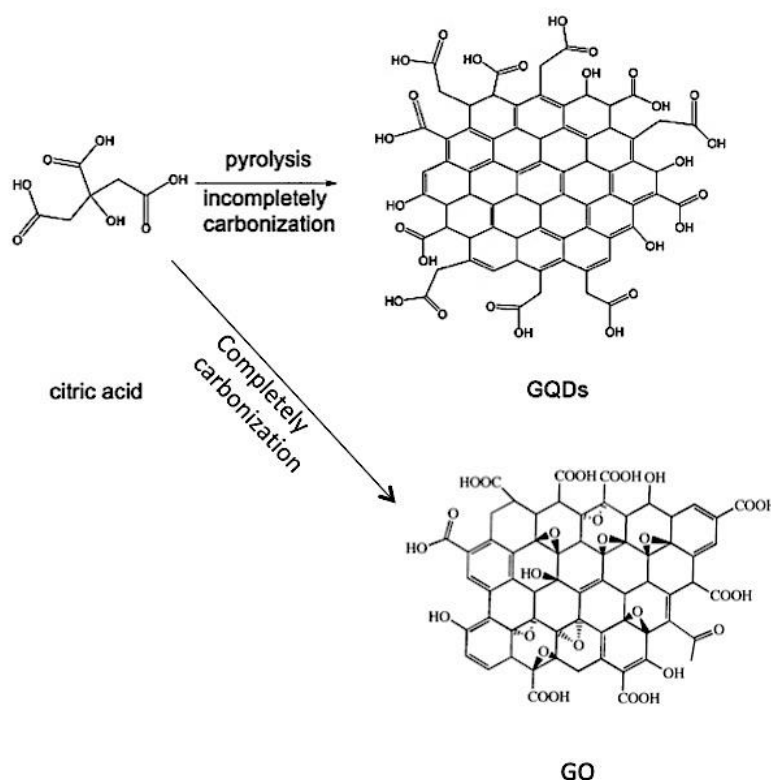
Figure 3 - Diagram for the synthesis of GQDs and GO.

Typically, GQDs have the edges rich in carboxylic acid functionalities, which improve dispersivity in water and can be used to bind surface-passivation reagents. Potentially, a variety of functionalized GQDs can be made through this approach, enabling luminescent probes with high quantum yield (QY) and able to recognize analytes.

The pyrolysis followed by hydro-exfoliation is one of the simplest methods for preparing GQDs. However, the corresponding luminescent QYs tend to be low when precursors and preparation conditions are not chosen carefuly. Doped GQDs with high QY can be obtained by pyrolyzing small organic molecules that contain heteroatoms, such as gluthatione (GSH), in their structures [77]. The composition of the solution, where the melted material is exfoliated, is also important to obtain high luminescent GQDs. Precursors that present organic functional groups such as chromophores may lead to products that offer properties that could be combined with the properties of graphene. In most cases, when organic molecules are covalently attached on the graphene, its extended aromatic character is perturbed, enabling the control of its electronic properties [78].

H. Sun *et al.* (2013) reported a photoluminescent probe for Cu^{2+} based on hydrothermal treatment of GQDs in a medium containing ammonia. The greenish-yellow photoluminescent GQDs, named as gGQDs and presenting low QY (2.5%), were hydrothermally treated in ammonia at 200ºC for 10h being, therefore, converted to amino-functionalized GQDs (afGQDs) with a higher QY (16.4%). Compared to other transition metal ions, Cu^{2+} has a higher binding affinity and faster chelating kinetics with N and O present on the afGQDs. Therefore, selectivity of afGQDs toward Cu^{2+} was found to be much higher than that of gGQDs. Furthermore, amination converted the surface charge of the GQDs from negative to positive, which makes easy for the afGQDs to be taken up by cells [79]. Li *et al.* (2011) have developed a simple and yet effective electrochemical strategy for generating N-doped GQDs with O-rich functional groups, which showed unique optoelectronic features distinctive from those of their N-free counterparts. In order to prepare N-GQDs, a modification of the previously reported electrochemical approach was made [80] by using, as the electrolyte, N-containing tetrabutylammonium perchlorate in acetontrile to introduce N atoms into the resultant GQDs. The N-GQDs were continuously produced by cyclic voltammetric scanning. The obtained N-GQDs were dissolved in the electrolyte solution while increasing the number of voltammetric scans cycles that led the solution color to change from colorless to yellow. Their unique luminescence properties indicate their potential for use in bioimaging and light-emitting diodes, among many other potential applications [81].

Ananthanarayanan *et al.* (2015) reported a simple and cost-effective method for the production of GQDs co-doped with N and P by carbonization and subsequent chemical exfoliation of a single precursor molecule - adenosine triphosphate (ATP). The dually doped GQDs showed high QY (~27.5%) and strong two-photon excitation with a two-photon absorption cross section. Carbonaceous micro-sheets resulting from ATP carbonization exhibited good catalytic properties towards oxygen reduction. When conjugated with transferrin, these heteroatom-doped GQDs have been employed to image and track transferrin receptors in live cells [82]. A simple approach for preparing GQDs with surface-passivated by

polyethylene glycol (GQDs-PEG) has been developed by Shen *et al.* (2012) (employing hydrothermal treatment of small graphene oxide (GO) sheets and polyethylene glycol (PEG). The obtained GQDs-PEG showed maximum emission at with 360 nm and QY of about 28.0% [83]. Liu *et al.* (2013) (presented a simple method to prepare GQDs with high luminescent QYs by a pyrolysis reaction of a mixture of citric acid (CA) and GSH as starting materials. The use of GSH in the preparation increased QY to 33.6% and improved the biological compatibility [77].

2.4.2
Physical and chemical proprieties of GQDs

The GQDs typically show strong optical absorption in the UV region, with a tail extending out into the visible range. D. Pan *et al.* (2010) reported that the photoluminescence spectra are generally broad and dependent on excitation wavelength. When the excitation wavelength is changed from 320 to 420nm, the photoluminescence peak shifts to longer wavelength and its intensity descreases rapidly, with the strongest peak excited at the absorption band.

The GQDs exhibit some size-dependency in terms of photoluminescence emission. Moreover, some other factors such as shape and edge functionalization could also affect their photoluminescence properties [84]. As a primary report, Eda *et al.* (2010) [85] used the density functional theory (DFT) to calculate the energy gap of $\pi-\pi^*$ transitions as a function of the number of fused aromatic rings. Since the band gap decreased gradually as the size of GQDs increased, sample mixtures of different particle size of GQDs presented different excitation and emission maxima.

It also should be noticed that the pH of the solution, where the GQDs are dispersed, also influence the photoluminescence intensity. As reported in literature, under alkaline conditions, the GQDs, obtained through simple hydrothermal approach, emitted strong photoluminescence whereas, under acidic conditions, the photoluminescence was nearly completely quenched. As pH is switched repeatedly between 13 and 1, the photoluminescence

intensity varied reversibly. Such reversible phenomenon was explained by Pan *et al.* (2010) based on proposed structural models and the photoluminescence mechanism of the GQDs. Under acidic conditions, the free zigzag sites of the GQDs are protonated, forming a reversible complex between the zigzag sites and H^+. Thus, the emissive triple carbene state is broken and becomes optically inactive. However, under alkaline conditions, the free zigzag sites are restored, thereby leading to the restoration of photoluminescence [71].

D. Pan *et al.* (2010) have also investigated the optical properties of these carbons nanoparticles in polar organic solvents showing that the UV-Vis absorption and photoluminescence spectra, observed in ethanol, methanol and glycol, were nearly the same as those observed in water. In acetone, however, these spectra changed remarkably as the absorption from 230 to 300 nm disappears and the 320 nm absorption feature shifted to 340 nm, while the photoluminescence maximum shifted from 400 nm to 430 nm and became broader. These results showed that the optical properties of the carbon nanoparticles are greatly influenced by acetone rather than by solvents with hydroxyl (OH) groups. This solvent effect, like the pH effect, can be related to the basic nature of the photoluminescent species in the nanoparticles because carbonyl (C=O) in acetone is a typical Lewis acid whereas hydroxyl in methanol, ethanol and glycol is a typical Lewis base [86].

2.5
Analytical methods using GQDs and QDs for Hg^{2+} sensing.

As mentioned, the properties of the QDs can be modified to some extent, making possible to adjust them according to the needs required for a given application. The presence of different ligands on the surface of the QDs can considerably alter their characteristics enabling the use of these nanoparticles in diverse analytical applications. Sensors based on the use of QDs are based on variations of the photoluminescent response of the nanoparticles in the presence of a given analyte. The analyte-QDs interaction may provide signal enhancement (increase in photoluminescent

intensity) or signal quenching, which is the most common quantitative analytical approach when using QDs as analytical probes.

J. Wang and Z. Li (2017) reported a facile one step synthesis of N-GQDs from the hydrothermal carbonization of fumaric acid in ammonia to be used as probe for Hg^{2+} detection. The luminescence response showed a linear decrease with increase of Hg^{2+} concentration in the range of 1.8×10^{-8} mol L^{-1} to 2.3×10^{-6} mol L^{-1}. The limit of detection of their method was calculated with a value of 5.9×10^{-9} mol L^{-1}. The feasibility of the developed method was investigated by analysing real water samples. The recovery experiments were performed by measuring the luminescence response of the sample after analyte fortification ranging from 97.5% to 102.0% [87].

On the other hand, Y. Yang *et al.* (2019) synthesized N, S-GQDs through hydrothermal process using critic acid and thioacetamide as the precursor and nitrogen/sulfur source, respectively. The luminescent probe was used for Hg^{2+} detection. Experimental studies indicated that non-radiative electron transfer between Hg^{2+} cations and N, S-GQDs caused dynamic luminescence quenching. The luminescence intensity of N, S-GQDs could be quenched after the addition of Hg^{2+} showing a good linear relationship ($R^2 = 0.991$) between the signal quenching and Hg^{2+} concentration in the range 1 to 30 nmol L^{-1}. Limit of detection of 0.27 nmol L^{-1} was obtained in aqueous solution. The applicability of the N,S-GQDs luminescent probe was investigated in real drinking water samples after fortification with the analyte with recovery ranging from 95 to 124% [88].

Srinivasan *et al.* (2016) developed a sensitive luminescent sensor based on the MoS_2 nanosheets/DNA/CDs nanoassembly towards the detection of Hg^{2+} in the environmental samples. The CDs presented strong luminescence, at 451 nm, after produced via one-step treatment from honey under low temperature carbonization. These CDs were nearly spherical, with average sizes around 2 to 4 nm. The luminescence of MoS_2 nanosheets/DNA/CDs nanoassembly enhanced with the increasing concentration of Hg^{2+} and the LOD was 1 nmol L^{-1}. Further, the signal response was linear ($R^2 = 0.98$) up to 10 nmol L^{-1} of Hg^{2+}. The present MoS_2 nanosheets/DNA/CDs nanoassembly was highly selective toward Hg^{2+} over a wide range of metal ions tested [4].

Another work explored ensemble between QDs (CdSe/ZnS) and AuNPs. Selectivity was based on the surface energy transfer in the QD/DNA/AuNP ensemble induced by Hg^{2+} and using this to detect this ion in water. The luminescence emission intensity was very sensitive to the change in the Hg^{2+} concentration and decreased as it increased. The luminescence quenching efficiency was quantified by the normalized net signal ($I = (F_0 - F)/F_0$, where F_0 and F were the luminescence intensity at 572 nm before and after Hg^{2+} addition). A linear correlation of the luminescence quenching was found within the Hg^{2+} concentration from 2 nmol L^{-1} to 60 nmol L^{-1}. The high sensitivity could be attributed to the efficient luminescence quenching by coupling several AuNPs to one QD. This sensor showed a LOD of 0.4 μg L^{-1} and the selectivity toward Hg^{2+} was demonstrated in an aqueous solution in the presence of the other metal ions [23].

Huang *et al.* (2013) described a time-gated fluorescence resonance energy transfer strategy employing water-soluble long lifetime fluorescence Mn-doped CdS/ZnS QDs and AuNPs to detect trace Hg^{2+} in aqueous solution. The nanoparticle ensemble was functionalized by two complementary single-stranded oligodeoxyribonucleotide (ssDNA), except for four deliberately designed thymine-thymine (T-T) mismatches. The QDs system acted as the energy-transfer donor, and the AuNP acted as the energy-transfer acceptor. When Hg^{2+} ions were present in the aqueous solution, DNA hybridization occurs because of the formation of T−Hg^{2+}−T complexes. As a result, the nanoparticle system are brought into close proximity, which induced energy transfer from QDs to AuNPs, leading to the quenching of luminescence with the increasing of the concentration of Hg^{2+}. Under the optimum conditions, the sensing system exhibited linear response within 1 and 10 nmol L^{-1} of Hg^{2+}. This sensor was used to detect Hg^{2+} in tap water, river water, and lake water fortified with Hg^{2+} [24].

By using two kinds of heteroatom doped carbon dots, one using 1, 2-ethylenediamine (CD-1) and other using N-(b-aminoethyl)-g-aminopropyl methyldimethoxysilane (CD-2), Yan *et al.* (2014) produced novel luminescent probes for detecting Hg^{2+} in pure aqueous solution within a broad pH range. Mercury ions were captured by the carboxyl groups of

these two kinds of CDs to form non-luminescent complexes (strong quenching). Both CD-1 and CD-2 exhibited high selectivity toward Hg^{2+}. The luminescence quantum yield and the detection ability of CD-1 was superior because of the electron-rich amino group with linear response ranging in the range of 1 to 12 µmol L^{-1} [31].

J. Li *et al.* (2018) developed a luminescent turn-on aptasensor towards the detection of Hg^{2+} based on CDs as donor molecules and MnO_2 nanosheets as acceptor molecules. The luminescent probe was fabricated through the conjugation with ssDNA on the surface of carbon dots. In the absence of Hg^{2+}, the carbon dots labeled with ssDNA were adsorbed on MnO_2 surface via Van der Waals force. The luminescence from CDs was then quenched by MnO_2 nanosheets via resonance energy transfer. As Hg^{2+} was introduced, the specific affinity interaction between ssDNA and Hg^{2+} detached the CDs-labeled ssDNA from MnO_2 surface because of the production of the T-Hg^{2+}-T complex, leading to the recovery of luminescence intensity. Under the specific reaction conditions, the signal intensity enhanced gradually with the increasing concentration of Hg^{2+} in the range from 2 to 200 nmol L^{-1}. In addition, the proposed strategy was successfuly applied in the determination of Hg^{2+} in water samples [89].

X. Yue *et al.* (2014) proposed the production of luminescent CDs by one-step hydrothermal treatment using apple juice as raw material. The luminescence of the produced CDs was quenched by Hg^{2+} with good selectivity. Based on this phenomenon, a selective and sensitive sensor was constructed for the detection of Hg^{2+} in phosphate buffer solutions (pH 7.0). The luminescence intensity varied in a linear way with Hg^{2+} concentration ranging from 5.0 to 100.0 nmol L^{-1} and the sensor was applied for the determination of Hg^{2+} in real water samples [33].

2.6
Flow Injection Analysis

Automatic methods of analysis have become well established, and automated analysers, either commercial, or constructed in-house, have become common features in most analytical laboratories. Automatic

analysers must be justified in terms of increased efficiency of laboratory operations, increased capacity and throughput of samples, and, most importantly, in terms of cost effectiveness [35]. Following the terminology established by the IUPAC (International Union of Pure and Applied Chemistry), automation is "the use of combinations of mechanical and instrumental devices to replace, refine, extend or supplement human effort and faculties in the performance of a given process, in which at least one major operation is controlled, without human intervention, by a feed-back system" [90].

In this context, the speed and simplicity of Flow Injection Analysis (FIA) offers significant potential advantages, in terms of analytical frequency, safety and metrological performance. In this respect, FIA offers the possibility of an on-line method optimization and most importantly the automatic analysis is carried out in a closed system; thus, materials which are toxic (such as mercury) or unstable in air can be more conveniently dealt with than by a manual method. FIA is a type of continuous flow analysis in which the flow is not segmented with air bubbles. An aliquot of sample solution is then introduced into the carrier stream, flowing through the FIA system, forming a zone, which is then transported toward a detector that continuously records the transient signal (any measured physical parameter) resulting from the passage of the sample zone through the flow cell (observation zone). The steps of such process is depicted in Figure 4: sample injection (phase 1), controlled dispersion of the injected sample zone (phase 2) and reproducible timing of its movement from the injection point to the detector (phase 3) and finally the injected sample is washed out from the detecting zone by the carrier (phase 4). A simplistic approach to FIA analytical systems is outlined in Figure 5.

This simple flow injection analyzer consists of a pump (P), which is used to propel the carrier stream through the tube; an injection port, through which a well-defined volume of a sample solution is injected, in a reproducible manner, into the carrier stream (phase 1); and a reaction coil (MC) in which the sample zone disperses and reacts with the components of the carrier stream (phase 2), forming a species which is sensed and recorded by a flow-through detector (phase 3). Then, the species formed is

washed out (phase 4) from the detector to a waste (W) container. A typical record output (time profile) has the form of a peak (Figure 6) allowing its height, width, or area to be related to the concentration of the species formed [91].
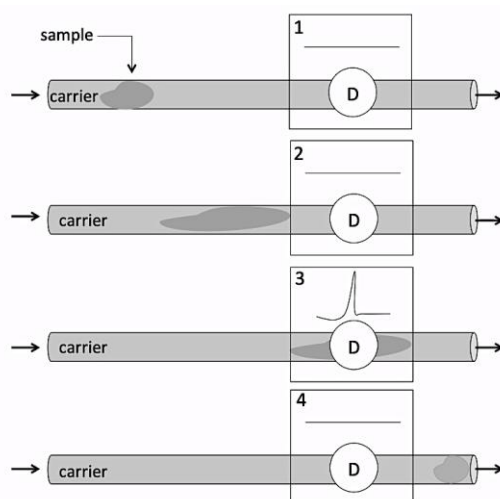
Figure 4 - Four phases of FI Analysis before and after sample is transported to detector (D). 1) Sample injection; 2) dispersion; 3) detection and 4) washout.
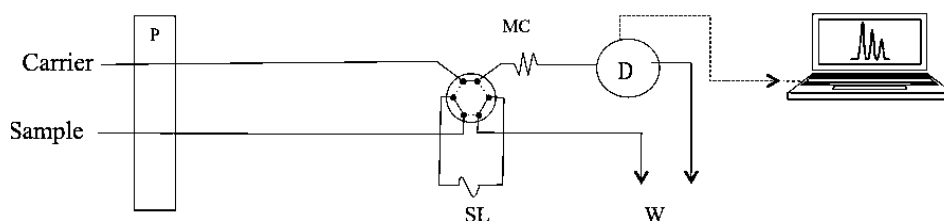
Figure 5 - Schematic diagrams of flow injection analysis. SL: Sample loop for loading tube with sample; D: Detector; P: Pump; MC: mixing coil and W: waste.
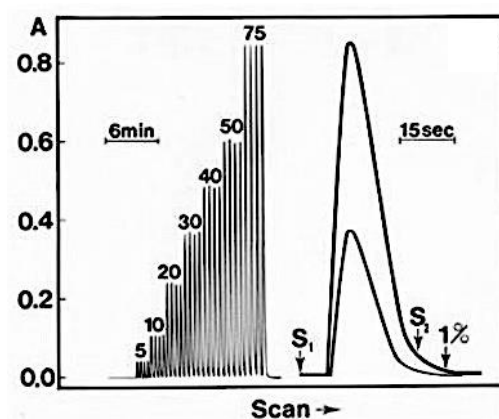
Figure 6 - A typical detector readout of a FIA system.

A key feature of FIA is that since all conditions are reproduced, dispersion of sample zone is controlled and kinetics of reaction is reproduced. Therefore, all samples are sequentially processed in the exactly same way during passage through the analytical channel. In addition, FIA is a microscale technique that consumes minute quantities of sample and reagents and therefore generates a very low of waste per assay.

3
Experimental procedures

3.1
Instrumentation

The FluoroMax®-4 spectrofluorometer (Horiba, Japan) was used to obtain luminescence spectra and for intensity measurements of the GQDs in batch assays as well as a detector of the FIA set up. A FIALab 2000 system (FIAlab Instruments, USA) was used for flow injection analysis. UV–vis absorption spectra were acquired on a Perkin-Elmer model Lambda 35 double beam spectrophotometer (Perkin-Elmer, UK). For method validation, mercury cold vapor (CV) measurements were made on a dedicated mercury CV multipass atomic absorption spectrometer (multipass-CV-AAS), model RA-915 (LUMEX, Russia), equipped with Zeeman background correction and connected to an RP-92 accessory for chemical reduction in aqueous solution. The Zeta potential measurements were performed on Zetasizer Nano ZS with MPT-2 titrator (Malvern, UK). For pH measurements, the pH-meter model MPA-210 (MS Tecnopon, model MPA-210, Brazil) with a glass membrane electrode combined with a reference Ag/AgCl (KCl saturated) was employed.

3.2
Reagents and materials and samples

Ultrapure water (18.2MΩ cm) was obtained from the Milli-Q gradient A10 ultra-purifier (Millipore, USA). Citric acid, glutathione (GSH), thiourea (TU), thioacetamide (TA), hydrochloric acid, sodium hydroxide, ethylene glycol-bis(β-aminoethyl ether)-N,N,N',N'-tetraacetic acid (EGTA) and standart stocks solutions of 1 mg mL^{-1} (Hg^{2+}, Co^{2+}, Fe^{2+}, Pb^{2+}, Cd^{2+}, Ni^{2+}, Cu^{2+}, Na^+, K^+, Mg^{2+} and Ca^{2+}) and 10 mg mL^{-1} (Zn^{2+}) were form Sigma-Aldrich (USA). Quinine sulfate were purchased from Fluka (Germany). Tin chloride ($SnCl_2$) was from Vetec (Brazil). Dialysis membranes (retained molecular weight of 3.5 kDa) were from Spectrum Laboratories Inc. (USA).

A standard reference material (SRM 1641c - Mercury in Water, certified value for Hg^{2+} of 1.47 mg L^{-1}) was from National Institute of Standards & Technology (USA). The mineral water was purchased from a local supermarket.

3.3
Procedures

3.3.1
Preparation of GQDs

The GQDs were prepared using the hydroexfoliation of the melted organic precursors, which consisted of citric acid (1.0 g) and 0.3 g of a chemical modifier: thiourea (TU), thioacetamide (TA) or glutathione (GSH) [77]. In order to enable a comparison, GQDs were also prepared using only citric acid. The solid mixture of precursors was heated in a beaker, to about 240 ºC, until the melted material reached a light brown color. Then, the pyrolyzed mass was poured into a beaker containing 50.0 mL of ultrapure water, at room temperature, forming a pale yellow mixture rich in the so-called graphene quantum dots (called original dispersions). These mixtures were then dialyzed for 24 h in using a dialysis membrane (3.5 kDa).

3.3.2
Spectrophotometric absorption and photoluminescence measurements

UV-vis absorption spectrophotometry was employed using 1000 nm min^{-1} scan rate, 10 nm spectral bandpass and small amounts of the dialysed original dispersions, diluted in water, placed on 10 mm optical path length quartz cuvettes. The scanned wavelength range was from 200 to 800 nm. The photoluminescence was measured after the original dialysed working dispersions of GQDs had been diluted in ultrapure water (1%v/v). A small aliquot of the working dispersions was transferred to a 10 mm optical path length quartz cuvette which had its final volume adjusted up to 3.0 mL with ultrapure water for blank measurements (solution without Hg^{2+}) with the

maximum excitation and emission wavelength indicated in Table 4, and spectral bandpass of 5 nm × 5 nm.

Table 4 - Maximum excitation and emission wavelength of the different carbon dots based dipsersions.

Probe	Excitation wavelengths (nm)	Emission wavelengths (nm)
GQDs	370	460
GQDs-GSH	350	430
GQDs-TU	350	435
GQDs-TA	328	414

Photoluminescence measured from GQDs working dispersions containing Hg^{2+} were normalized by their respective reference signals (L_0), which is the signal measured from working dispersions in absence of Hg^{2+}, in order to establish an increasing relationship between normalized signal (L_0/L) and the concentration of Hg^{2+}, with K_s (quenching constant) as the sensitivity factor, as indicated in Equation 1.

$$L_0/L = 1 + K_s[Hg^{2+}]$$

Equation 1

In order to measure photoluminescence, the volume of mercury standard solution was added before the working dispersion had their volume adjusted with ultrapure water, to 3.0 mL. When including any additional component, the addition was also made before adjusting the final volume with ultrapure water.

3.3.3
Quantum yield determination

Photoluminescence quantum yields (Φ) of the GQDs were obtained comparing their integrated fluorescence spectrum intensity with the same quantity for a reference standard solution (QY = 55%) of quinine sulfate (1.0 x 10^{-4} mol L^{-1}) [92], prepared in sulfuric acid (0.5 mol L^{-1}). The measurements were performed using by exciting both GQDs and quinine

sulfate at 345 nm. The integrated photoluminescence intensity was calculated by measuring the entire area under the emission spectrum. In order to minimize the self-absorption, the absorbance of the measured solution/dispersion was kept below 0.10. The QY was then calculated according to the Equation 2:

$$\phi_f^i = \frac{F^i f_s n_i^2}{F^s f_i n_s^2} \; \phi_f^s \qquad\qquad \text{Equation 2}$$

Where ϕ_f^i and ϕ_f^s are the photoluminescence QY of the sample and that of the standard, respectively (the subscript f is used because in most cases fluorescence is the phenomenon evaluated). The F^i and F^s are the integrated intensities (areas) of spectra from sample and standard, respectively; f_x is the absorption factor, that is, the fraction of the incident light that is absorbed ($f_x = 1 - 10^{-Ax}$, where A = absorbance); the refractive indices of the sample and reference solution are n_i and n_s, respectively. In this experiment, the diluted GQDs were dispersed in deionized water (n_i = 1.00) and the diluted solution of quinine sulfate was dissolved in 0.5 molL^{-1} sulfuric acid (n_s = 1.33).

3.3.4
Preparation of standard solutions and working dispersions

Working dispersions of GQDs (the so called analytical probes) were prepared by transfering 1.0 mL of the dialyzed original dispersion into a 10.0 mL volumetric flask. The volume was then adjusted with ultrapure water. When batch analysis was performed, the standard or sample solution was added before adjusting final volume with ultrapure water. Mercury standard stock solutions, as well as other metal ions mentioned in this work, were prepared by the dilution of 1.0 mg mL^{-1} of the standard solution with ultrapure water. Standard solutions of lower concentration were prepared by dilution of the stock solutions also with water. The EGTA stock solution (1.0 x 10^{-2} mol L^{-1}) was prepared by dissolving an appropriated mass in

water. The $SnCl_2$ (2% v/v) solution, used for determination of Hg^{2+} by multipass-CV-AAS, was prepared by dissolving 20 g of the salt in 100 mL of concentrated HCl. This solution was heated in order to evaporate half of its volume aiming the elimination of mercury contamination found in the HCl solution and avoiding contamination of the system. After cooling the solution, water was added to complete volume to 100 mL. Before use, the solution was placed on a glass bottle washer to be purged with nitrogen gas for 15 min.

3.3.5
Preparation of samples solutions

Water samples were a locally purchased mineral water. The sample for FIA assay was a simulated mineral water with low content of alkaline and alkaline earth ions. Sample was fortified with Hg^{2+} at 375 μg L^{-1} and with the following ions: Na^+ (6 μg L^{-1}), K^+ (10 μg L^{-1}), Ca^{2+} (10 μg L^{-1}) and Mg^{2+} (6 μg L^{-1}).

3.3.6
Zeta-potencial titration

The zeta potential (ζ) of the GQDs dispersion was determined as a function of pH using NaOH and HCl standardized solutions as titration agents. Initially, three NIST certified buffers (pH 4, pH 7 and pH 10) were used to calibrate for MPT-2 titrator. Then, 5 mL of the original GQDs-TU dispersion were transferred to the titration vessel of the MPT-2 titrator, and then 0.20 mL of KCl solution (3.0 mol L^{-1}) was added and stirred in order to adjust the ionic strength. The pH, ranging from 2 to 9, was adjusted with NaOH (0.1 mol L^{-1}) and HCl (0.01 mol L^{-1} and 0.1 mol L^{-1}). The Smoluchowski equation [93] was employed to calculate the zeta potential. All measurements were carried out at 25 ºC.

3.3.7
Flow injection analysis system

The FIA system is shown schematically in Figure 7 and the chosen parameters for flow analysis are given in Table 5. The pump and injection valve were fully controlled by FIALab for Windows 5.0 software (FIALab Instruments) and the FluoroMax®-4 spectrofluorimeter was used as the detector. The operating parameters such as pump speed, sample introduction volume, tubing diameter and length were optimized in order to obtain the better sensing condition.

Table 5 – Optmized operating parameters employed in FIA system

Parameter	Value
Flow rate	2.5 mL min^{-1}
Tubing internal-diameter	0.8 mm
Sample volume	326 µL
Mixing Coil length	2 m
Integration time	0.2s
Excitation wavelength	350 nm
Emission wavelength	435 nm

The manifold used in this study (schemed in Figure 7 and 8) consisted of a peristaltic pump, a narrow tube; an injection valve; and a micro reactor (mixing coil) in which the sample zone disperses and interacts with the components of the carrier stream, forming the product (GQDs-TU-Hg^{2+}) that is sensed by a flow-through detector and recorded. Identical Teflon tubes (0.8 mm i.d) were used to maintain identical flow rates in each feedline. An 80 µL quartz flow-through cell (Hellma, Germany) with optical pathlength 10 mm was employed for photoluminescence detection cell.
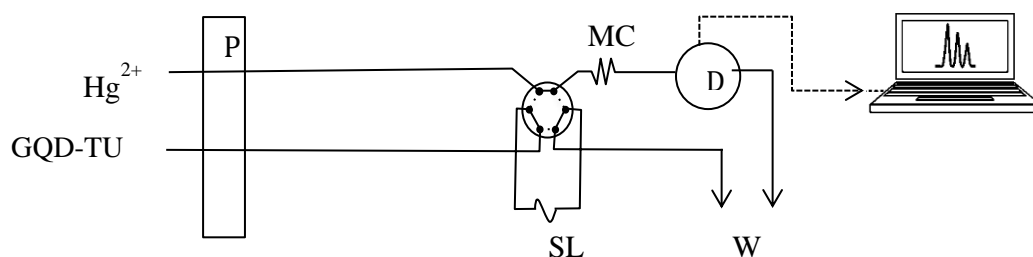
Figure 7 - Schematic diagram flow for indirect determination of Hg^{+2} using GQDs-TU as photoluminescent probe. SL: Sample loop for loading tube with sample; D: Detector; P: Pump; MC: mixing coil and W: waste.

In order to provide a better analytical scheme, the probe dispersion is pumped by the peristaltic pump (P) through the designated tubing, loading the sample loop (SL). A bypass loop allows passage of the carrier solution (in this case the solution containins sample before and after standard addition) when the injection valve is in the load position. Both carrier solution (sample containing Hg^{2+}) and working dispersion (GQD-TU probe dispersion) are constantly pumped to a waste container (W) until injection valve is in injection position. Once the injection valve is switched to injection position, the probe changes its course and introducing a volume, adjusted by the sampling loop, to the carrier stream flowing to the reaction coil, to allow better interaction between analyte and nanoparticles. The flow carried the formed analytical zones toward the detector (D) and then to a waste container.
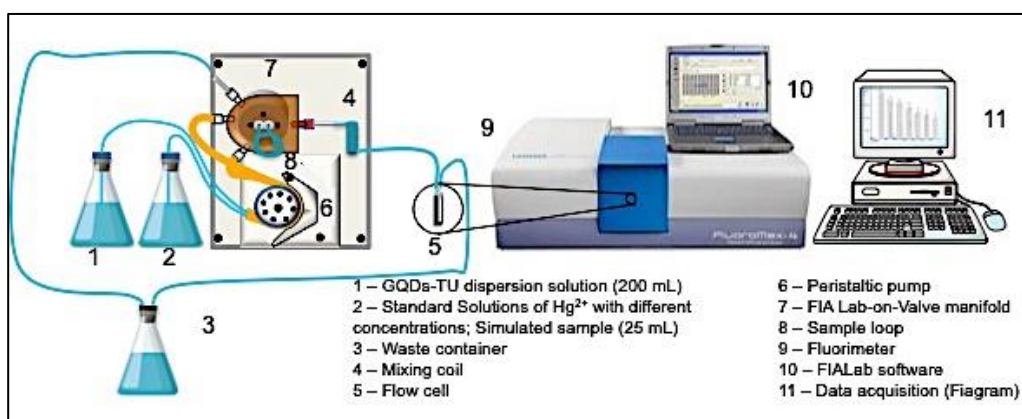
Figure 8 - Flow injection analysis system

3.3.9
Analytical procedure for determination of Hg^{2+} by multipass-CV-AAS

For the determination of the mercury in the samples, 10 mL of the sample were added to the glass reaction cell containing 3 mL of $SnCl_2$ (20% m/v). This reaction cell was an instrument reduction accessory, where a continuous airflow was constantly passed through the solution to enable fast Hg^{2+} reduction and the transferring of the formed Hg^0 to the multipass cell of the CV-AAS spectrometer. Zeeman background correction was used, operation was the continuous acquisition mode and the 253.6 nm line (from a $6^1S_0 - 6^3P_1$ transition) was monitored.

4
Results and discussion

Three different carbon nanoparticles were produced by hydro-exfoliation in pure water using melted mixtures of citric acid and sulfur-containing compounds. These sulfur-containing compounds were glutathione (GSH), thiourea (TU) or thioacetamide (TA) and they were used to produce sulfur functionalizations onto nanoparticles that supposedly provide more efficient interaction with mercury, enabling disturbances in the optical properties of nanoparticles themselves. Carbon nanoparticles produced only with citric acid (hydro-exfoliated in alkaline medium) was used as a reference, in terms of photoluminescence, since it is a well-known route to produce the luminescent nanomaterials referred in this text only as GQDs. The different carbon nanoparticles were evaluated using different techniques and their interaction with Hg^{2+} were compared in terms of the variation in photoluminesce, aiming to select one to be used in the analytical probe (probe dispersion).

The carbon nanoparticles dispersions, obtained from the hydro-exfoliated melted (semi-carbonized) compounds, were dialyzed and the dialyzed dispersions were denominated "original dispersions". As the concentration of carbon nanoparticles in these original dispersions cannot be directly accessed, it was decided to measure their total carbon content, enabling reference values to quantitatively indicate the content of carbon present in the diluted aqueous dispersions that were used to detect Hg^{2+} (referred in this text as "probe dispersions"). Total carbon in the original dispersions varied from 61 µg g^{-1} (GQDs) and 127 µg g^{-1} (GQDs-TA and GQDs-GSH) as seen in Table 6.

Table 6 - Total carbon content measured in different original dispersions of carbon nanoparticles and the ones expected in the diluted dispersions used to evaluate the influence of Hg^{2+}.

Nanoparticle	Total carbon in original dispersion [a] ($\mu g\ g^{-1}$)	Total carbon in probe dispersion containing Hg^{2+} [b] ($\mu g\ g^{-1}$)
GQDs	61	0.033
GQDs-TA	127	0.13
GQDs-TU	107	0.11
GQDs-GSH	127	0.048

[a]– hydro-exfoliated melted material after dialysis (original dispersion).

[b] – original dispersion after dilution with water.

4.1
Optical characteristics of the different GQDs

Extinction spectra in the UV-Vis range (Figure 9) were obtained for the different original dispersions. In all cases, broad exticticion profile, covering the range from 200-300 nm, was observed. This feature is characteristic of semiconductor quantum dots and attributed to π-π* transition of C=C conjugated of sp^2 carbon and to functional groups at the edge of the quantum dots. Except for GQDs-TU, a well-defined extinction band, indicative of the first excitonic, is found at higher wavelength range with peak maxima varying from 308 nm (GQDs-TA) to 350 nm (GQDs-GSH). For GQDs-TU, the extinction band was wider and no clear spectral structuring was observed.

The photoluminescence emission and excitation spectra have been obtained after dilution, in water, of the original dispersion and presented with normalized maximum values in Figure 10. In all cases, excitation spectra presented FWHM of about 100 nm with maximum wavelength varying from 328 to 370 nm. The feature of the excitation band (symmetry and FWHM) suggests that the produced carbon-sp^2 clusters are fairly uniform in size. All of the emission spectra from the sulfur-containing nanoparticles were blue-shifted when compared to the one obtained only using citric acid (GQDs). They presented single maxima that vaired from 414 nm (GQDs-TA) to 440 nm (GQDs-TU) and their Stokes shifts (λ_{em} - λ_{ex}) were 80 nm for GQDs-

GSH, 86 nm for GQDs-TA and 96 nm for GQDs-TU, all of them similar to the reference GQDs (90 nm).
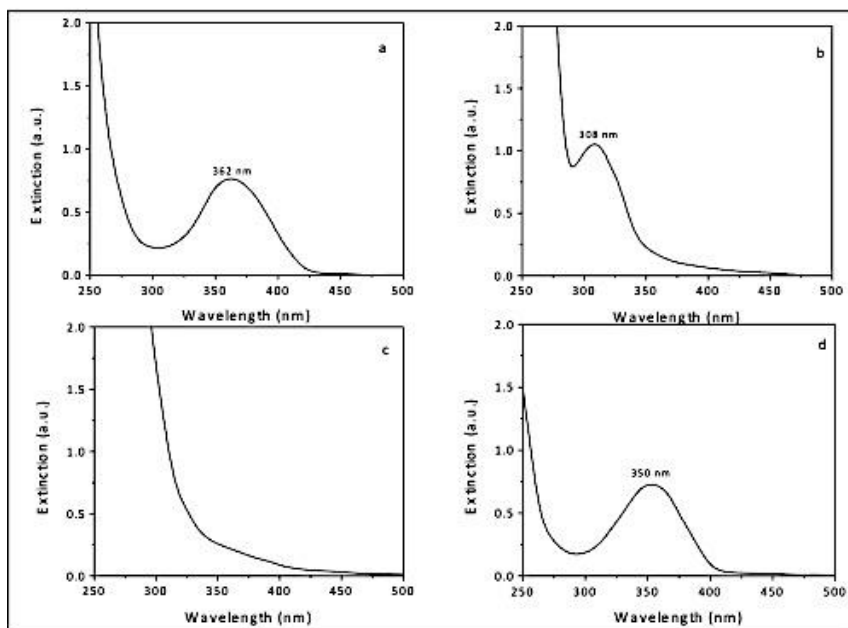
Figure 9 - Extinction spectra from the original GQDs dispersions: a) GQDs; b) GQDs-TA, c) GQDs-TU, d) GQDs-GSH
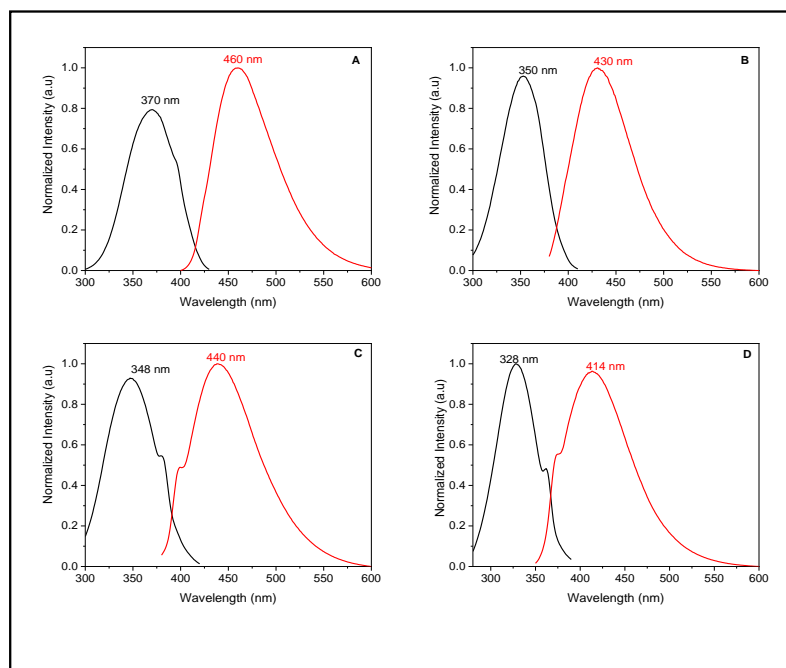
Figure 10 - Photoluminescence spectra of the produced GQDs obtained with only citric acid (in alkaline medium) and with mixtures containing citric acid (in water) and their maximum emission wavelengths (λ_{em}) and maximum excitation wavelengths (λ_{ex}): A) GQDs obtained only with citric acid (370/460 nm); B) GQDs obtained with glutathione (350/430) nm; C) GQDs obtained with thiourea (348/440 nm); D) GQDs obtained with thioacetamide (328/414 nm).

In terms of photoluminescent quantum yield (QY), significant differences were found when comparing the different luminescent carbon nanoparticles. The GQDs produced from citric acid (in alkaline medium) presented QY value of 8.0% whereas lower QY values were found for GQD-TU (2.2%) and GQD-TA (1.8%), indicating that any produced functionalizations were not able to produce an electron donating effect that would improve efficiency of the nanoparticle excitonic recombination. In contrast, nanoparticles obtained using GSH presented very high QY (55.4%) probably due to the nature of the functionalizations produced by the presence of groups –SH in GSH, compared to the -C=S present in TU and TA, and the presence of amino groups combined with carboxylic acid groups that are absent in TU and TA (compound in which primary amines are not assocated with carboxylic acid).

4.2

Effect of Hg^{2+} on the photoluminescence of the different GQDs

In order to study the effect produced by Hg^{2+} on the photoluminescence measured from the diluted GQDs dispersions, a reference signal (equivalent to about 70% of the detection system scale before saturation) was established to allow the selection of the volume of the original GQDs to be diluted in water. After dilution, the total carbon content in each of these diluted dispersions (probe dispersions) varied from 0.033 to 0.13 µg g^{-1} (as seen in Table 6) and their pH were 9.3 (GQDs), 4.7 (GQDs-GSH), 5.0 (GQDs-TA) and 4.1 (GQDs-TU).

As the maximum concentration of Hg^{2+} in water depends upon the pH of the medium, it is expected a prompt precipitation of Hg^{2+} when added to the dispersion of GQDs (prepared in basic condition). Despite that, the experiment was performed in order to observe and compare the effect in terms of measured photoluminescence. Taking into consideration a system at pH 5.0, the maximum concentration of Hg^{2+} would be in the order of 1 µmol L^{-1} (calculated from K_{ps} = 3.6 × 10^{-26} at 25 °C). Therefore, the concentration of Hg^{2+} in this experiment was fixed at 0.25 µmol L^{-1} (equivalent to 50 µg L^{-1}).

Photoluminescence from the diluted GQDs dispersions were measured before and right after the addition of a small aliquot of a Hg^{2+} stock solution, chosen to enable the final concentration of Hg^{2+} established for the study. It was observed that the addition of Hg^{2+} produced photoluminescence quenching for all of the different GQDs with no spectral shifting associated with signal decreasing. The relative quenching factors can be seen in **Erro! Fonte de referência não encontrada.** as L_0/L where L_0 is the original luminescence from the nanoparticle dispersion and L is the one measured right after the addition of the metal ion. The least effective in terms of quenching was the GQDs-GSH, with only 14% of signal decreasing. For the other GQDs, a more significant quenching was immediately achieved in the following order: GQDs > GQDs-TU > GQDs-TA.
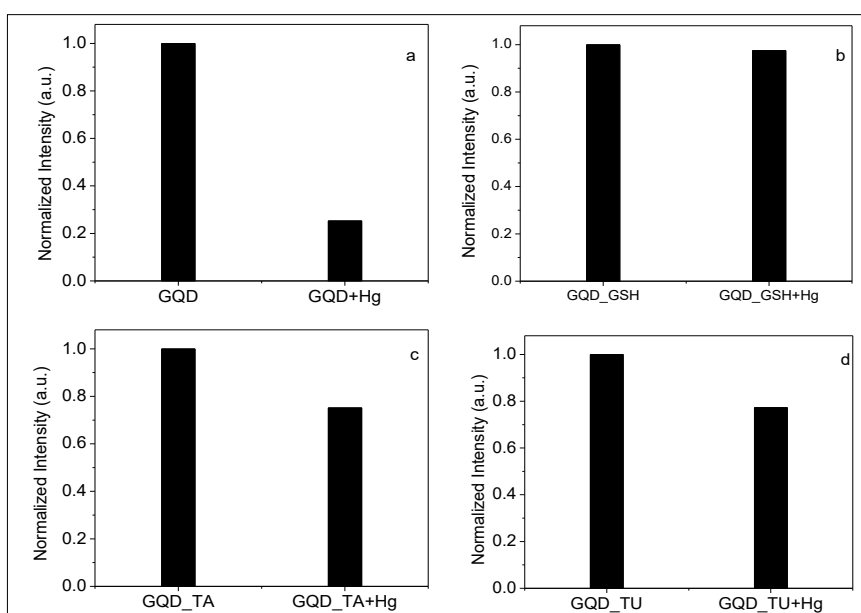
Figure 11 - Normalized photoluminescence quenching from different GQDs dispersions in (a) absence and in the presence of (b) Hg^{2+} at 50 μg L^{-1}): A) GQDs; B) GQDs-GSH; C) GQDs-TA; D) GQDs-TU. L_0/L where L_0 is the original luminescence from the nanoparticle dispersion and L is the one measured right after the addition of the metal ion.

By comparing the probable impact caused by the use of sulfur-containing compounds in the production of GQDs, it seems that GSH, which contains a thiol group, may have produced –SH functionalization that is less

effective in interacting with Hg^{2+} when compared to functionalizations produced by using precursos containing -C=S, where sulfur would be more exposed to interact with Hg^{2+}. However, it is important to point out that citric acid, which would not produce functionalization neither with sulfur nor with nitrogen containing groups, was the nanoparticle that better interacted with Hg^{2+}, producing the larger signal quenching factor. However, this result could probably be explained by other mechanism based on the behavior of the added ion in alkaline medium. As Hg^{2+} is added into the alkaline dispersion, $Hg(OH)_{2(aq)}$ is readily formed and deposited onto the surface of carbon nanoparticles (acting as nucleation sites). In this way, a layer of $Hg(OH)_{2(s)}$ passivates the surface of the GQDs, quenching its photoluminescence.

The photoluminescence quenching effect produced by Hg^{2+} was monitored over time (right after the addition up to 40 min after mixing Hg^{2+}) as depicted in Figure 12. It was found that photoluminescence from GQDs-GSH took about 5 minutes to reach a stable profile with random signal oscilation. In contrast, for the GQDs-TA and GQDs-TU dispersions, the signals were promptly quenched and their intensities remained stable during the entire period of the study. In the case of GQDs, photoluminescence continuously decreased over the 40 minutes duration of the experiment, never reaching a stable value. This is one indication of the nanoparticle surface passivation as a relatively slow deposition of $Hg(OH)_{2(s)}$ (from the formed $Hg(OH)_{2(aq)}$) onto the surface of the GQDs is expected.

In order to acquire more information on how efficient these GQDs would be as probes for Hg^{2+}, a test was made to evaluate the effect produced by the presence of selected ions of toxic potential (all of them at a concentration equivalent to about 0.25 μmol L^{-1}). These selected ions and their concentrations were: Co^{2+} (15 μg L^{-1}); Zn^{2+} (16 μg L^{-1}); Pb^{2+} (52 μg L^{-1}); Cd^{2+} (28 μg L^{-1}); Ni^{2+} (15 μg L^{-1}). The results are summarized as L_0/L in Figure 13, where the quenching effect produced by Hg^{2+} is also shown for comparative purposes. Dispersion produced only from citric acid (hydro-

exfoliated in alkaline medium) was not tested as its alkaline pH is not appropriate to keep in solution most of the ions tested.
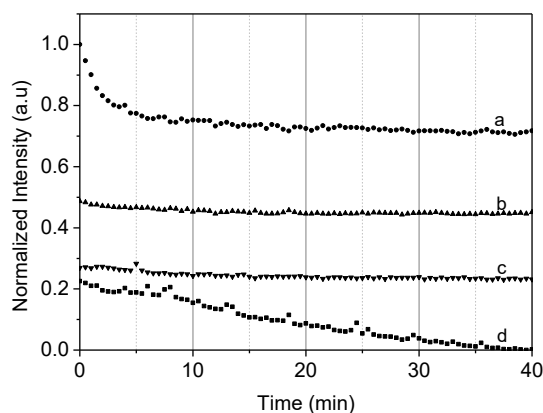
Figure 12 - Intensity of the quenched photoluminescence produced by Hg^{2+} (at 50 µg L^{-1}) over time: a) GQDs-GSH; b) GQDs-TA; c) GQDs-TU; d) GQDs.
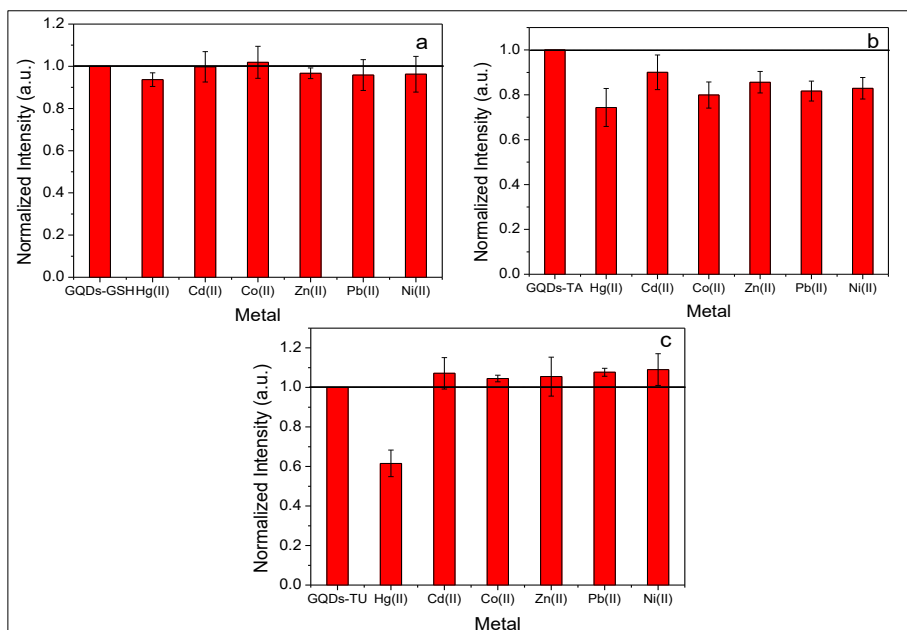
Figure 13 - Normalized photoluminescence quenching from different GQDs dispersions in absence (blank) and in the presence of different metal ions: Hg^{2+} (50 µg L^{-1}); Co^{2+} (15 µg L^{-1}); Zn^{2+} (16 µg L^{-1}); Pb^{2+} (52 µg L^{-1}); Cd^{2+} (28 µg L^{-1}); Ni^{2+} (15 µg L^{-1}). a) GQDs-GSH; b) GQDs-TA; c) GQDs-TU. The L_0 is the original luminescence from the nanoparticle dispersion and L is the one measured right after the addition of the metal ion.

The result indicated that GQDs-GSH (Figure 13A) were not immediately affected by the presence of the ions used in this study, since signal quenching factors were non-sigficative. As for the GQDs-TA (Figure 13B), the presence of all of the ions promoted signal quenching almost as intense as the one observed by Hg^{2+}. In contrast, the quenching effect

produced by the tested ions on the photoluminescence measured from the GQDs-TU dispersion was insignificant compared to the effect observed for Hg^{2+}. These results indicated that the nanoparticle produced using citric acid and thiouera was the one that showed the best potential to be used as a probe for Hg^{2+} (Figure 13C). Therefore, further studies were made only with this nanoparticles (GQDs-TU) in order to understand the interaction between them and Hg^{2+} and to adjust the conditions to enable the probe to be evaluated in the analytical point of view.

4.3
Evaluation of the GQDs-TU dispersion

The morphology of the GQDs-TU original dispersion was evaluated using field emission scanning electron microscopy (FE-SEM), operating in the transmission mode, resulting in the image shown in Figure 14. The image was processed using the program Image-J in order to obtain the statistical distribution of nanoparticle parameters. Most nanoparticles were in the range from 25 nm to 40 nm although nanoparticles can be found in the range from 10 nm to 70 nm (insert of Figure 14). The aspect ratio histogram (Figure 15A) indicated that most nanoparticles present the ratio between the shortest axis and the longest axis (orthogonal) varying between 1.1 and 1.3 and the maximum difference between axis is 1.6. Taking into account that perfect circularity is indicated by 1, the experimental aspects indicate that most nanoparticles are fairly circular (circularity between 0.75 - 0.95) as seen in the histogram of Figure 15B.
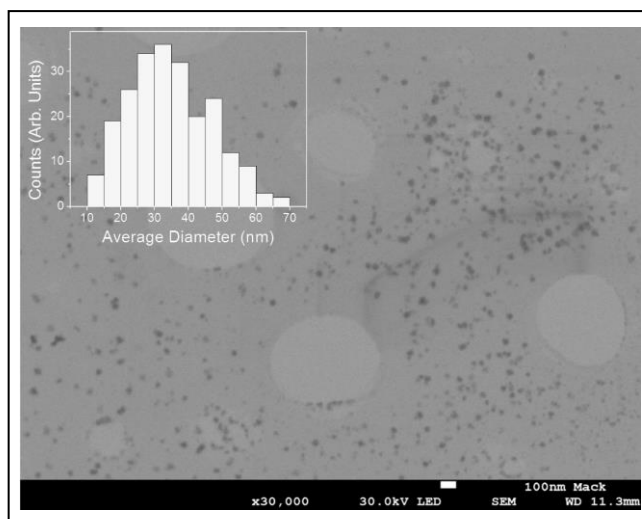
Figure 14 - FE-STEM images and average diameter of the original dispersion of GQDs-TU.
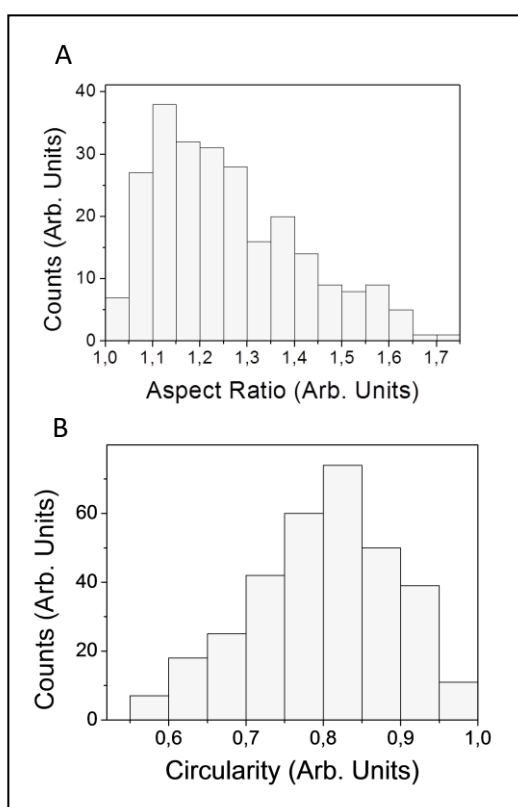
Figure 15 - Histograms for the aspect ratio and circularity of GQDs-TU produced from microscopic image in Figure 14.

A study was performed to evaluate the profile of the photoluminescence measured from dispersions of GQDs-TU in function of the pH (in the range from 2.0 to 9.0) trying to find a correlation with

nanoparticle surface charge. The final pH values were adjusted by the addition of small aliquots of either HCl or NaOH solutions (at 0.01 or 0.01 mol L^{-1}).

It was observed that as the pH of the dispersion increased, the larger was the measured photoluminescence (Figure 16a) with a noticiable spectral blue shift, of about 20 nm, occurring when pH of the medium changes from a more acidic condition to a less acidic condition (at pH above 4.0) as seen in Figure 16b. In the pH range from 2 to 4 (the acid range appropriate to keep Hg^{2+} in solution), only a small increment in measured photoluminescence was found (18 % more intense at pH around 4 than at around 2). A strong increasing was observed as the pH varied from 5 to about 8, and then stabilizing up to pH 8.8.
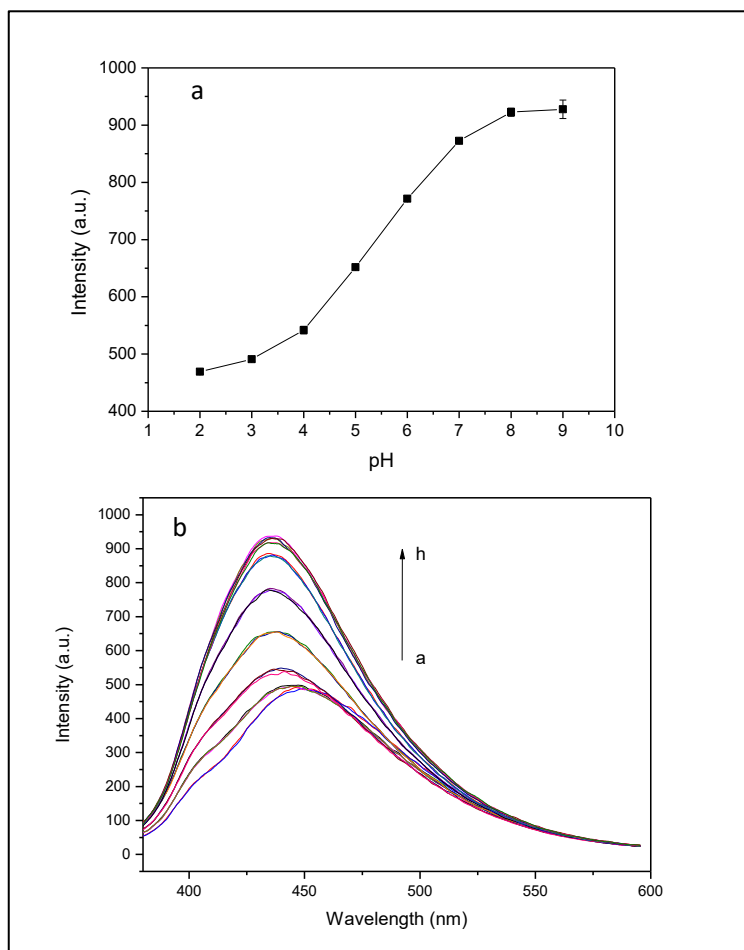
Figure 16 - a) Influence of pH on the photoluminescence intensity from GQDs-TU dispersion and b) spectral profiles at different pH values from a to h (a: 2; b: 3; c: 4; d: 5; e: 6; f: 7; g: 8; h: 9).

In order to understand such behavior, ξ potentials of nanoparticles were also measured (Figure 17) along the pH change. It was found a strong correlation of surface charge and photoluminescence as the low charged particles, at pH 2.2 (ξ = +2.5) and 3.2 (ξ = -3.3), becomes increasingly negative as the acid condition changed from pH 3.9 (ξ = -10.5) to pH 8.8 (ξ = -41.4). It could be inferred that carboxylic acid functionalization (produced due to the use of citric acid) becomes deprotonated (more negative) as the pH increased leading to a more efficient repulsion between nanoparticles thus favoring quantum confinement. At more acidic conditions, carboxylic acid groups are protonated leading to aggregation of carbon nanoparticles (a termodinamically favored process) with formation of hydrogen bonds. The aggregation decreases quantum confinement and the photoluminescence produced through CB-VB electron recombination.
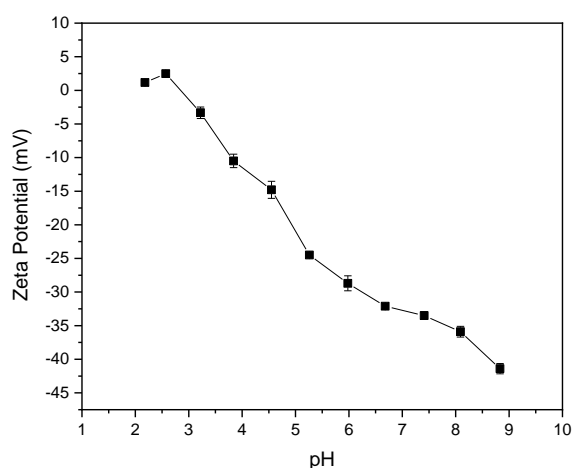
Figure 17 - Superficial charge (as zeta potential) of GQDs-TU in function of the pH

4.4
A brief study on the interaction between GQDs-TU and Hg^{2+}

The nature of the interaction between the GQDs-TU and Hg^{2+}, producing the photoluminescence quenching effect, was evaluated through a series of experiments made at controlled temperature (Figure 18). For this study, the photoluminescence quenching was monitored in function of the increasing concentration of Hg^{2+} (from 0 to 30 µg L^{-1}) under four different

temperatures (from 20 to 35 °C). It was observed that the photoluminescence quenching was more effective at lower temperatures as the sensibility of the quenching curve at 20 °C was almost four times higher the one observed at 35 °C. This behavior is a characteristic of static quenching as the increasing of temperature decreases the stability of any long-term interaction between the nanoparticles and the analyte ion.
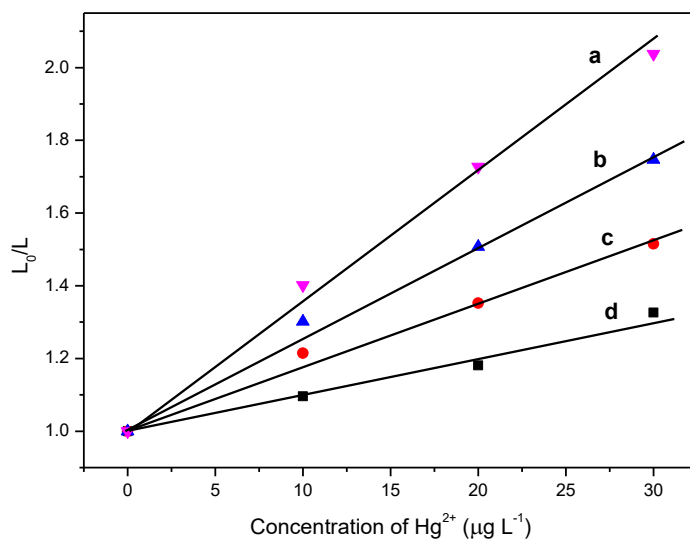
Figure 18 - Normalized curve for GQDs-TU in the presence of increasing concentrations of Hg^{2+} in aqueous system (with sensibilities in parenthesis) at a) 20 °C (3.6×10^{-2} L μg^{-1}) b) 25 °C (2.5×10^{-2} L μg^{-1}) c) 30 °C (1.8×10^{-2} L μg^{-1}) d) 35 °C (1.0×10^{-2} L μg^{-1}).

The result is an indication that a long-term species, referred as GQDs-TU-Hg^{2+} is formed not necessarily with a defined stoichiometry since a carbon nanoparticle may have diverse sites for the interaction with Hg^{2+}. It is probable that photoluminescence quenching is due to an electron withdrawal that makes electrons unavailable for excitonic recombination, similar to what has been observed in systems containing GQDs-GSH and Fe^{3+} reported previously in literature [32]. However, it could not be ruled out any other effect related to external heavy atom effect in relaxing excited states involved.

The hipothesis of the formation of a non-luminescent GQDs-TU-Hg^{2+} species is reinforced by measurements of ξ potentials of the dispersions (at pH 4.0 and at pH 7.0) in the presence of Hg^{2+}. In both cases, the presence of Hg^{2+} produced a change of the net surface charge towards positive

values (less negative values). At pH 4, ξ potential of $-(26.0 \pm 0.6)$ mV was found while the addition of Hg^{2+} changed ξ potential to $-(14.9 \pm 1.7)$ mV. At pH 7.0, the ξ potentials measured in dispersions before and after the addition of Hg^{2+} were respectively $-(37.5 \pm 0.4)$ mV and $-(21.8 \pm 2.4)$ mV.

4.5
Analytical characteristics

4.5.1. The analytical response of GQDs-TU in presence of Hg^{2+}

Based on the results achieved in the previous studies, the conditions for the GQDs-TU probe dispersion were chosen in order to allow the detection of Hg^{2+} (summarized in Table 7). A batch analysis study was performed by measuring the photoluminescence from the probe dispersion (inside a cuvette) after the addition and mixing of increasing volumes (from 10 to 40 μL) of a 10 mg L^{-1} Hg^{2+} stock solution as seen in the series of spectra of Figure 19A. The normalized plot, with the photoluminescence decreasing normalized by the original photoluminescence (L_0/L), showed a linear trend in function of the analyte concentration over the tested concentration range (10 μg L^{-1} to 40 μg L^{-1}) with a coefficient of determination (R^2) of 0.998 as seen in Figure 19B. The curve equation was $y = 0.0241$ (L μg^{-1}) $x + 1.0$.

The limit of quantification (LOQ) was 10 μg L^{-1} (0.050 μmol L^{-1}) and it was calculated as a concentration of Hg^{2+} capable to reduce the probe photoluminesncence by a signal value equivalent to 10s (where s is the standard deviation of the measured signal from original probe dispersion). The limit of detection (LOD) was 3 μg L^{-1} (0.015 μmol L^{-1}).

Table 7 - Conditions for the GQDs-TU probe dispersion

Condition	Value
Volume of original GQDs-TU dispersion/ Volume of intermediary dispersion	1.00mL/10.00mL
Intermediary dispersion volume/ probe dispersion volume	30μL/ 3mL
Carbon content in probe dispersion	0.11 μg g^{-1}
pH (original)	3.9 – 4.1
Temperature	Ambient Temperature (~20ºC)
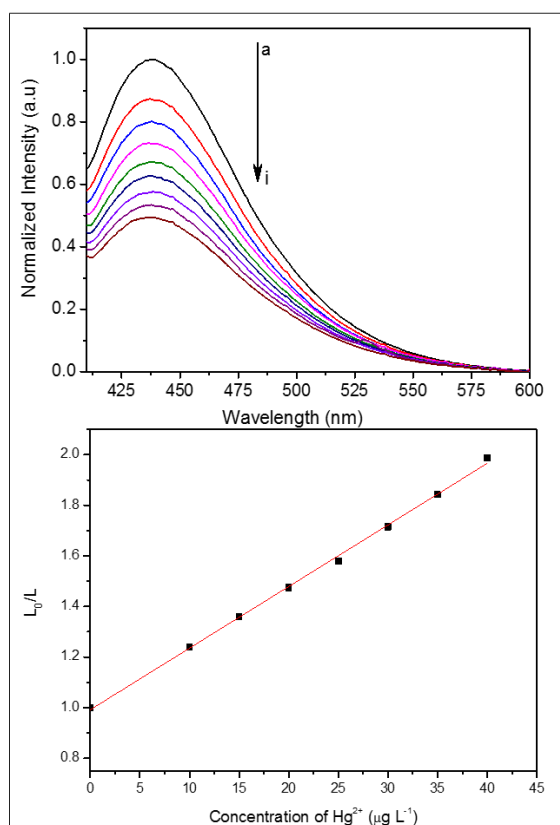
Figure 19 - (A) Photoluminescent response from the GQDs-TU probe dispersion in the presence of increasing concentrations of Hg^{2+}: a) 0, b) 10 c) 15, d) 20, e) 25, f) 30, g) 35, h) 40 μg L^{-1}. (B) Normalized analytical curve for the GQDs-TU photoluminescence quenching in presence of Hg^{2+}: $y = 0.0241$ (L μg^{-1}) $x + 1.0$ (R^2 = 0.998).

Precison was calculated at two different concentration levels (at 20 and at 40 μg L^{-1}). Considering signal variation reported as L_0/L, precision was a percent value based on Equation 3, where $s_{(L_0/L_i)}$ is the combined

standard deviation and L_0/L_i is the normalized photoluminescence value obtained by the addition of Hg^{2+} at a specific concentration.

$$precision = \frac{s_{(L_0/L_i)}}{L_0/L_i} \times 100 \qquad \text{Equation 3}$$

The $s_{(L_0/L_i)}$ was calculated according to Equation 4, where L_0 is the average original signal from the probe and L_i is the average signal from the probe in the presence of Hg^{2+} at a specific concentration and s_{L_i} and s_{L_0} are the standard deviations based on four replicates. The precison at 20 μg L^{-1} was 0.51 % while at 40 μg L^{-1} it was 0.60 %.

$$s_{(L_0/L_i)} = \frac{L_0}{L_i}\left[\left(\frac{s_{L_0}}{L_0}\right)^2 + \left(\frac{s_{L_i}}{L_i}\right)^2\right]^{\frac{1}{2}} \qquad \text{Equation 4}$$

4.5.2. Study of interferences

4.5.2.1. Evaluation of inteferences

Considering that alkaline and alkaline earth metals can be present in water samples, a study was performed to evaluate the influence of Na^+, K^+, Mg^{2+} and Ca^{2+} on the photoluminescence measured from the probe. These four main ions are generally present in drinking water at relatively high concentrations, which may tipically vary from 1 mg L^{-1} up to 10 mg L^{-1} while others, such as Sr^{2+} and Ba^{2+}, are usualy in the range below 0.1 mg L^{-1}. Specification for six alkaline and alkaline earth ions in five different commercial mineral waters are displayed in Table S1 (supplementary material).

Spectroscopic standard solutions of Na^+, Mg^{2+}, Ca^{2+} (1000 mg L^{-1} in HNO_3 1%) and of K^+ (10.000 mg L^{-1} in HNO_3 1%) were used to prepare more diluted solutions from where aliquots were added to the GQDs-TU probe dispersion. Photoluminescence quenching imposed by these ions can be seen in Figure 20. For Mg^{2+} and Ca^{2+}, maximum quenching was achieved with about 2000 μg L^{-1} (Figure 20A and Figure 20B). At these concentrations, quenching for Mg^{2+} and Ca^{2+} were respectively 39.4 % and 38.8 % of the GQDs-TU probe original signal. Larger quantities of Mg^{2+} and

Ca^{2+} did not produce any further decreasing in photoluminescence. In the case of Na$^+$, maximum quenching effect was found in the presence of 6000 μg L^{-1} (Figure 20D), promoting quenching that resulted in 43.8% of the GQDs-TU probe original signal. In contrast, photoluminescence intensities measured in the presence of K$^+$, even above 1000 μg L^{-1}, produced a very small decreasing of the original signal of the GQDs-TU probe (Figure 20C).
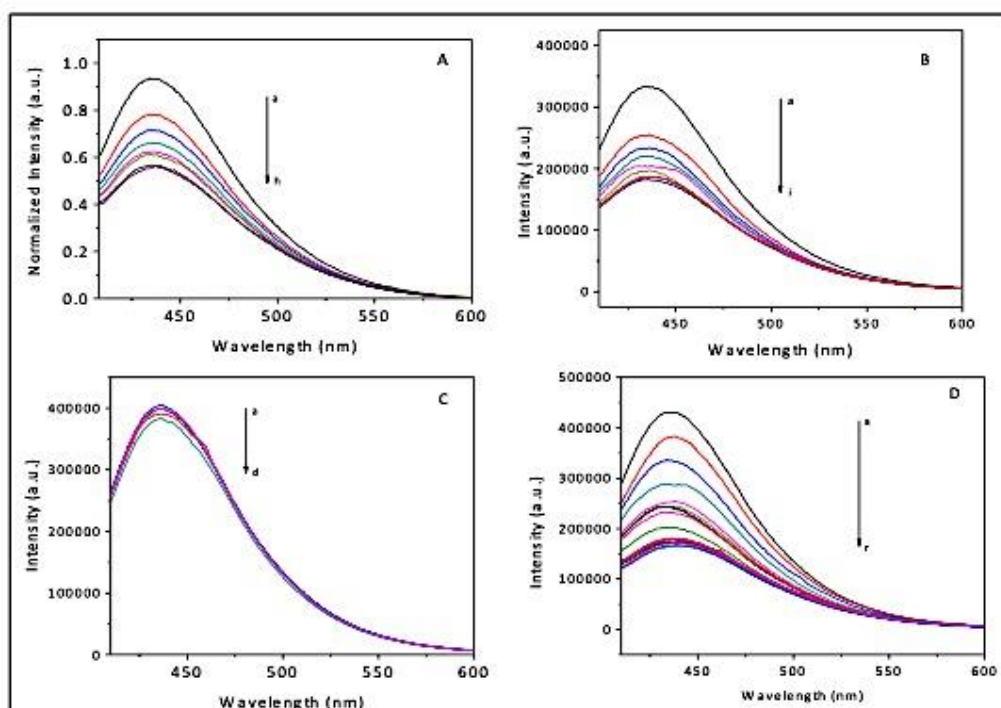
Figure 20 - Quenching effect produced by the presence of alkaline and alkaline earth elements on the GQDs-TU probe: A) Mg^{2+} from a to h: 300, 600, 900, 1167, 1500, 2000, 2500μg L^{-1}; B) Ca^{2+} from a to i: 330, 660, 1000, 1330, 1667, 2000, 2330, 2667 μg L^{-1};C) K$^+$ from a to d: 100, 300, 600, 900μg L^{-1}; D) Na$^+$ from a to i: 150, 300, 600, 900, 1167, 1500, 2000, 2500, 3330, 4000, 6000, 6667, 7000, 7500, 8000, 8500 μg L^{-1}.

A comparison of the quenching factor produced by each of the tested ions, at 2000 μg L^{-1} (chosen to ensure maximum quenching effect) is shown in Figure 21. It is interesting that the increasing magnitude of the quenching effect is in the inverse order of the ionic radius (shown in parenthesis): Na$^+$ (154 pm) > Mg^{2+} (160 pm) > Ca^{2+} (197 pm) >> K$^+$ (227 pm).
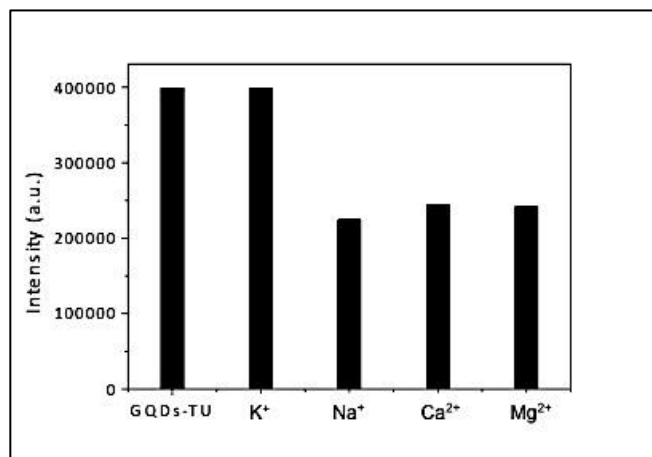
Figure 21 - Relative photoluminescence intensities from GQDs-TU dispersions in the presence of K⁺, Na⁺, Ca²⁺ and Mg²⁺ at a 2000 μg L^{-1} concentration level. Blank intensity is the original signal measured from the GQDs-TU dispersion.

4.5.2.2. Evaluation of the use of a chelating agent to mitigate interferences from alkaline and alkaline earth ions.

One of the possible strategies to minimize interferences imposed by alkaline and alkaline earth ions is to mask them, using a chelating agent, in order to make them unavailable to interact with the GQDs-TU. If selective masking is succesfull, the signals measured in a reference probe containing the chelating agent would be statisticaly similar to the ones from probes containing the alkaline and alkaline earth ions along with the chelation agent.

Literature reports the efficiency of various chelating agents in binding alkaline earth cations. However, as Hg^{2+} is the target analyte, ideally masking should not be made at alkaline pH, condition in which chelating agents as ethylene glycol-bis(β-aminoethylether)-N,N,N',N'-tetracetic acid (EGTA) and eltylenediamino tetracetic acid (EDTA) are more effective.

A simulation using the MAXCHELATOR calculator [94], that uses database of constants from the National Institute of Standard and Technology (NIST), indicated that EGTA is very inefective in chelating Mg^{2+} and Ca^{2+} (close to 100% free ions at pH 4 and even at pH 6, taking into account initial concentrations of 10 μg L^{-1} for Ca^{2+} and μg L^{-1} for 5 Mg^{2+}). In Figure 22, the free ions plot simulations are shown for pH 4, pH 6 and pH

8. Similar results would be expected for EDTA.
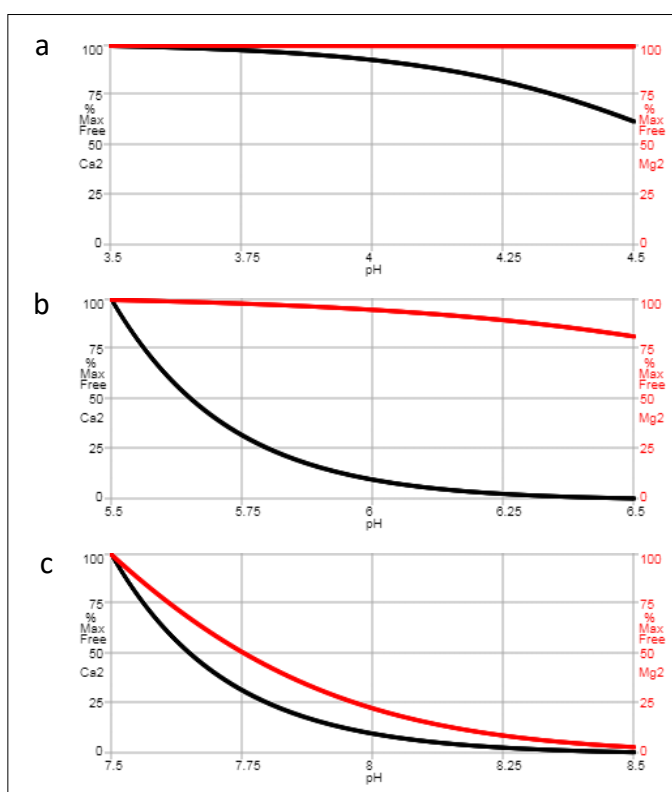
Figure 22 - Simulated pH plot from the MAXCHELATOR software used to estimate free metals content in an EGTA solution (0.01 mol L^{-1}) in a system containing required to complex 25μM Ca^{2+} and 15μM Mg^{2+} at a pH from 6 to 8 @25°C.

Very effective chelation with EGTA would be achieved for both alkaline earth ions only in the range between pH 8.3 and pH 8.5 (Figure 22C), which are not appropriate to keep Hg^{2+} in solution. However, in fact, the adjustment of EGTA concentration itself in the probe dispersion causes a pH increase that affect the probe response as indicated in Figure 23.
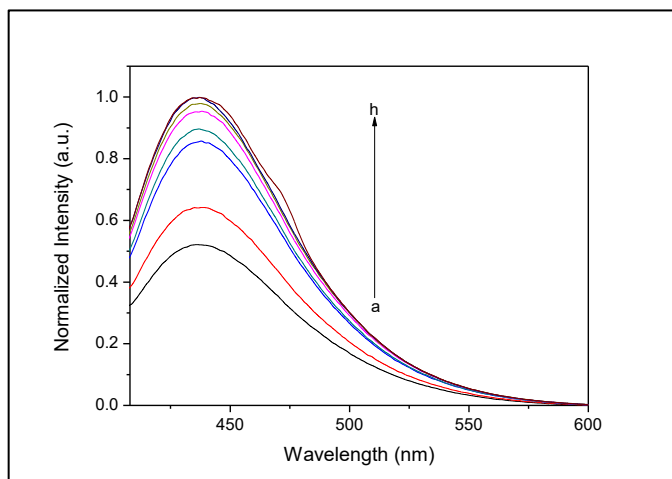
Figure 23 - Normalized photoluminescent intensity of GQDs-TU in presence of increasing concentrations of EGTA: a) 0 (pH 4.0); b) 17 μmol L^{-1} (pH 4.8); c) 33 μmol L^{-1} (pH 5.3); d) 50 μmol L^{-1} (pH 5.9); e) 67 μmol L^{-1} (pH 6.2); f) 83 μmol L^{-1} (pH 6.6); g) 100 μmol L^{-1} (pH 7.0); h) 113 μmol L^{-1} (pH 7.7).

4.5.2.3. Evaluation of matrix buffering to compensate interferences from alkaline and alkaline earth ions

When sample matrix solutions are made identical to the ones of the calibration standards (matrix matching), any change in analytical signal can be only due to the changing in analyte concentration and both translational and rotational type interferences are impossible to occur [95]. Matrix buffering or interference saturation is one type of matrix matching used when the source of interference is known.

The underlying principle of matrix buffering is the addition to both, test solutions and standard solutions, of an overwhelming concentration of the substance responsible to the matrix effect (interference) [95]. In the case of this work, saturation with interferents would be applied to the probe dispersion in order to guarantee signal changes only due to the standard addition of analyte. It has been demonstrated that maximum signal decrease is achieved in the presence of 2000 μg L^{-1} of either Ca^{2+} or Mg^{2+} and in the presence of 6000 μg L^{-1} of Na$^+$ (as seen in Figure 20). In order to evaluate the possibility to perform analysis under matrix buffering conditions, a study was conducted using GQDs-TU probe dispersions fortified with either Ca^{2+} or Mg^{2+} ions at the indicated concentration that

imposed maximum interference effect. To these dispersions, increasing concentrations of Hg^{2+} were added, which produced a further quenching effect that was proportional to the increase of the concentration of analyte (Figure 24).
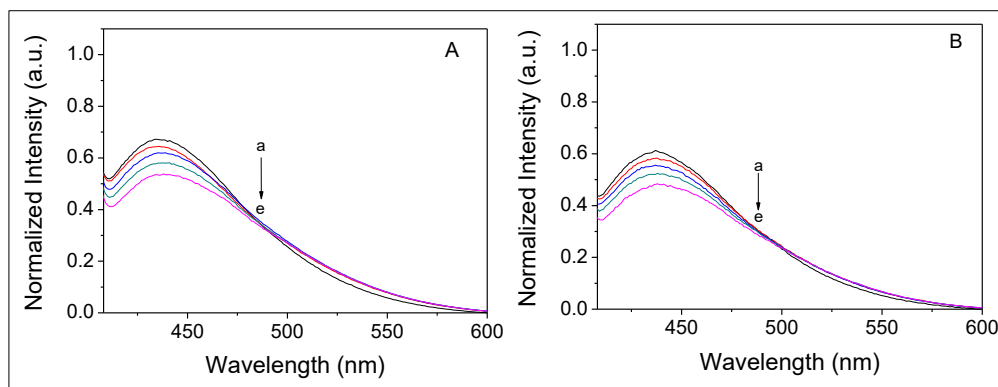
Figure 24 - Photoluminescent response of the GQDs-TU towards Hg^{2+} in interferent buffering conditions: A) 2000 μg L^{-1} of Ca^{2+}; B) 2000 μg L^{-1} of Mg^{2+}; Increasing concentrations of Hg^{2+}: a) 0 μg L^{-1}; b) 300 μg L^{-1}; c) 600 μg L^{-1}; d) 1200 μg L^{-1}; e) 2400 μg L^{-1}.

At matrix buffering conditions, the normalized analytical curves were contructed using L_0/L in function of the concentration of Hg^{2+} (Figure 25). In both cases, sensibilities of the curves were similar: 1.1×10^{-4} L μg^{-1} (in buffering conditions with Mg^{2+}) and 1.0×10^{-4} L μg^{-1} (in buffering conditions with Ca^{2+}). However, compared to the sensibility obtained using the probe without matrix buffering, sensitivity was 100 times lower, severely degrading LOD and LOQ, which were respectively 35 μg L^{-1} and 120 μg L^{-1}. Linearity of the response was also affected as R^2 values degraded to values below 0.98.
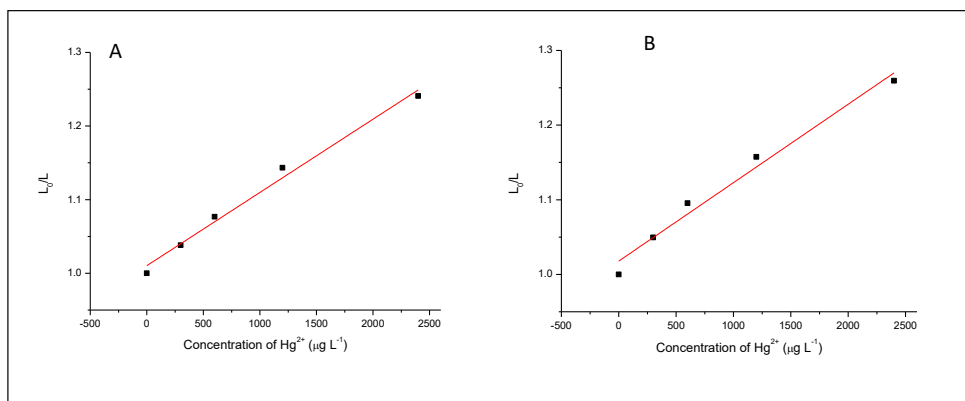
Figure 25 - Normalized analytical curve for the GQDs-TU photoluminescence quenching in presence of Hg^{2+} under matrix buffering conditions for Mg^{2+} (at 2000 μg L^{-1}) and for Ca^{2+} (at 2000 μg L^{-1}). Curve equation in the presence of Mg^{2+}: $y = 1.10 \times 10^{-4}$ (L μg^{-1}) + 1.02 (R^2 = 0.959) and curve equation in the presence of Ca^{2+}: $y = 1.01 \times 10^{-4}$ (L μg^{-1}) + 1.01 (R^2 = 0.974).

The experiment under buffering conditions with Na^+ (at 6000 μg L^{-1}) was also performed. It was observed that further addition of Hg^{2+} did not provide a specific signal response with measured photoluminescence producing small non-sistematic variations upon increasing amounts of Hg^{2+} (Figure 26). This is a extreme case of interference that forces the use of a strategy to separate Hg^{2+} from the sample prior to determination.
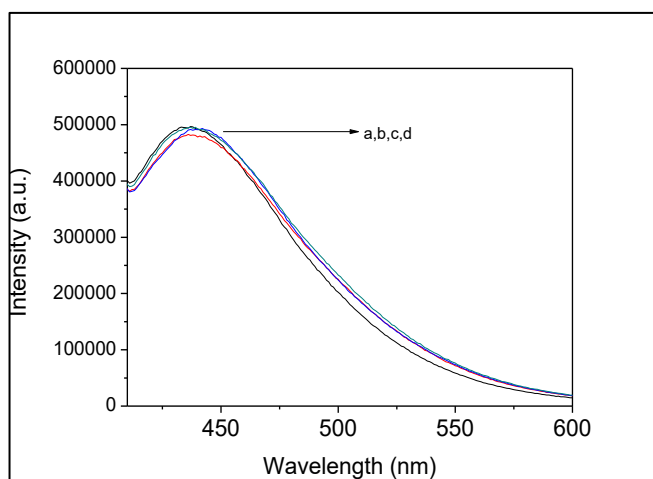
Figure 26 - Photoluminescent response of the GQDs-TU towards Hg^{2+} in interferent buffering conditions for Na^+ (at 6000 μg L^{-1}) Increasing concentrations of Hg^{2+}: a) 0 μg L^{-1}; b) 300 μg L^{-1}; c) 600 μg L^{-1}; d) 1200 μg L^{-1}; e) 2400 μg L^{-1}.

The experiment with increasing concentrations of Hg^{2+} was repeated in a probe dispersion containing 2000 $\mu g\ L^{-1}$ of Ca^{2+} and Mg^{2+} besides 6000 $\mu g\ L^{-1}$ of Na^+. In this case, interference was found to be as severe as the one produced by the presence of Na^+ alone (Figure 27).
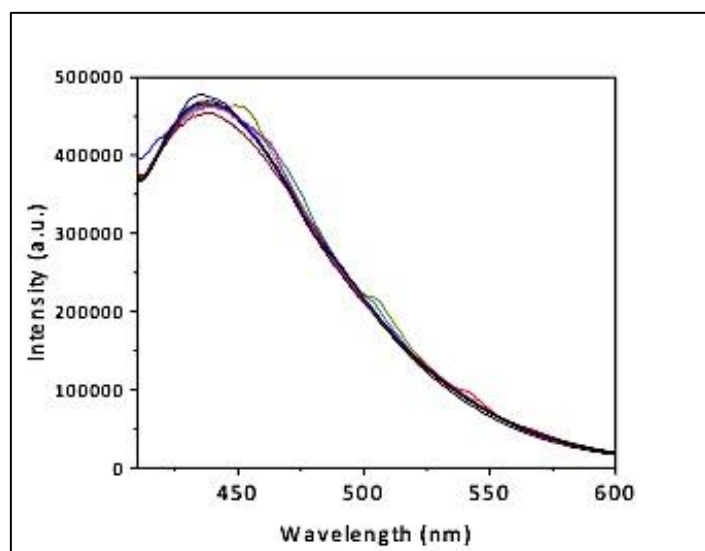
Figure 27 - Photoluminescent response of the GQDs-TU towards Hg^{2+} in interferent buffering conditions including Na^+ (at 6000 $\mu g\ L^{-1}$); Mg^{2+} (at 2000 $\mu g\ L^{-1}$) and Ca^{2+} (at 2000 $\mu g\ L^{-1}$). Increasing concentrations of Hg^{2+}: a) 0 $\mu g\ L^{-1}$; b) 300 $\mu g\ L^{-1}$; c) 600 $\mu g\ L^{-1}$; 1200 $\mu g\ L^{-1}$; 2400 $\mu g\ L^{-1}$.

4.6
Application of the method in regime of flow injection analysis

4.6.1. Flow injection analysis manifold setup adjustments

In order to adapt the use of the GQDs-TU analytical probe into flow analysis regime, a brief optimization of conditions was made to provide proper analytical response. First, a flow rate of 2.5 mL min^{-1}, which corresponded to 50% of the maximum pump velocity, was used since it provided best peak time profile resolution between sequential injections made every 15 s. At higher flow rates, such as 5.0 mL min^{-1}, peak profile did not to reach baseline before the next injection.

Sample volume (S_v) was also chosen aiming to provide a sharp peak profile. Two volumes were tested in function of the length of the sampling loop as indicated: 5 cm loop (providing injection of 25 μL of solution) and 60

cm loop (providing 325 μL of solution). The injection of 25 μL produced very small peaks, which would affect sensitivity of determination. In contrast, the use of 325 μL enabled intense and sharp peaks, proper to enable good analytical response. Longer sampling loops were not tested, as larger sampled volumes tend to produce larger analytical zones, thus severe dispersion affecting peak resolution.

Methods based on chemical reactions involving the analyte are often used in flow analysis. Such reactions take place inside the tubbing of the FIA systems between injection and detection points. Therefore, tubbing length plays a crucial role in a proper generation of analytical signal and it is set, along flow rate, to provide enough time for uniform mixing of reactants and time for reaction to proceed (not necessarily until its completion). When the sample is injected into a carrier solution containing a reactant, the chemical reaction does not proceed uniformly throughout the entire sample zone. It starts at the edges of the sample zone (where first contact between analyte and reactant occurs) then progressing towards the center as the sample zone undergoes dispersion and the mixing with carrier solution continues. A similar effect would be expected in the determination of Hg^{2+} using GQDs-TU, as probes, as photoluminescence variation relies on an effective contact between analyte and nanoparticle. In such situations, larger zones tend to produce double-humped peaks (or in the case of this work, does not produce an effectively measurable quenching effect) that would not normally occur if the monitored species depended only upon physically driven dispersion [96].

Since a relatively large S_v was used in this work, laminar dispersion often cannot provide sufficient mixing between the injected GQDs-TU probe and the analyte present in the flow carrier. The use of a reaction coil minimizes such undesirable effects by providing a more effective mass transport by means of flow disturbances (radial mixing). Two different lengths for the reaction coil were tested. The short lenght coil (30 cm) was not long enough to provide proper interaction and significant variation in measured signal. In contrast the longer mixing coil (200 cm), combined with the flow rate of 2.5 mL min^{-1}, provided significant signal variation yet keeping peak profile sharp enough to allow large analytical frequency (volume

introduced per minute) set by the 15 s interval between injections. The FluoroMax®-4 spectrofluorometer was used as detection system and setup conditons for detection are indicated in Table 5 including the integration time of 0.2 s that provided a proper duty cycle for the analysis.

Under the conditions established for FIA, previously summarized in Table 5, different dilutions of the original dispersions were used to prepare the diluted ones used to be intruced into the FIA system. Three dilution factors were used (10 times; 20 times and 100 times) and the result is shown in the fiagram displayed in Figure 28 with maximum signal normalized to 1.0. The fiagram indicates reproducibility of signal and proper resolution of probe peak time profiles. The dilution factor of 100 times was chosen since it was the one used in batch analysis and changing the proportion between carbon nanoparticles and analyte (within an optimized range) can influence interaction, leading to unknown behavior that affect analytical response.
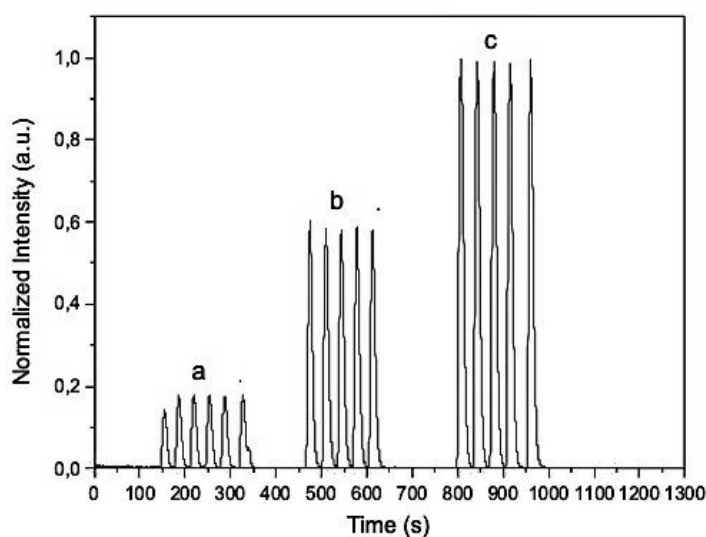
Figure 28 - Fiagrams obtained by injecting three different probe aqueous dispersions prepared from different dilution factors of the original dispersions: a) 100 times; b) 20 times and c) 10 times).

4.6.2
Analytical figures of merit in FIA.

Analytical information through FIA was produced by first measuring photoluminescence form the introduced volume of GQD-TU probe in to

water as carrier flow ("blank"). Then, the water was changed to analyte standard solutions, as carrier, to construct the analytical curve after introduction of GQDs-TU whose photoluminescence is affected (quenched) by the Hg^{2+} in the carrier. For each analyte concentration, the carrier was allowed to flow for approximately 1 minute, for proper flushing of the previous standard solution, before introduction of probe. The analyte standard solutions, used as carriers, presented Hg^{2+} concentrations varying from 100 μg L^{-1} to 900 μg L^{-1} and the resultant fiagram (with four replicate probe additions for each analyte concentration) is shown in Figure 29.
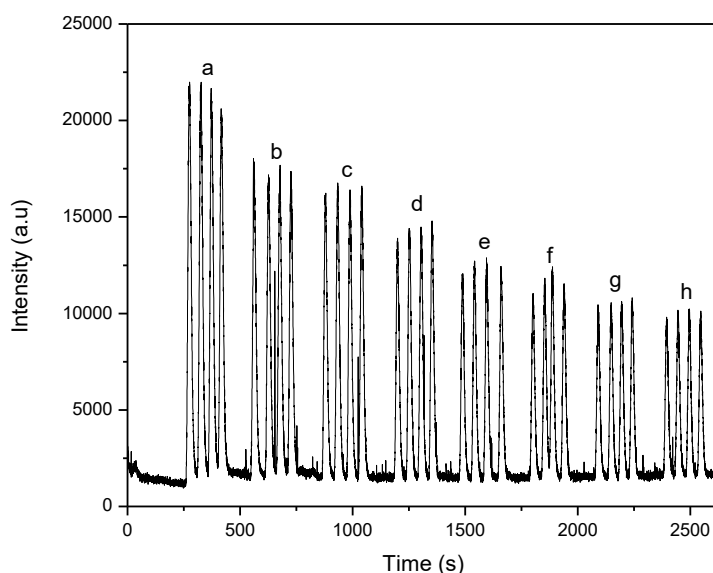
Figure 29 – Fiagram showing the analytical responses of the analytical curve for Hg^{2+} by using GQDs-TU as photoluminescent probe. Standard solutions of Hg^{2+} at a) 0; b) 100; c) 150; d) 300; e) 450; f) 600; g) 750; h) 900 µg L^{-1}

The normalized analytical curve (Figure 30) presented a linear response considering L_0/L as a function of Hg^{2+} concentration. LOD and LOQ values were calculated based on respctively $3s_b/m$ and $10s_b/m$ with s_b based on ten blank measurements. LOD and LOQ along with parameters of the analytical curve are presented in Table 8.
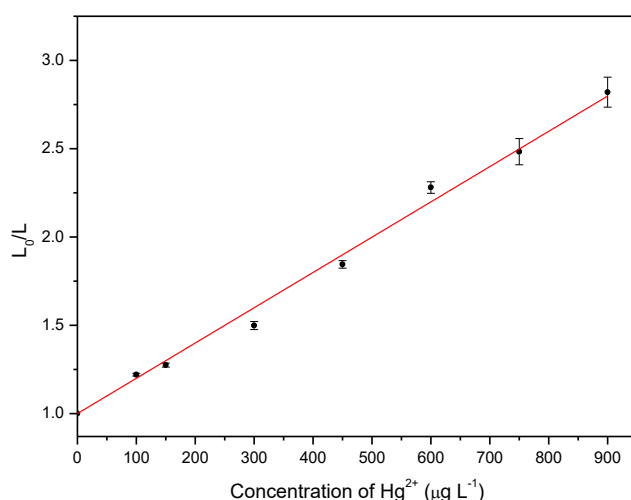
Figure 30 - Normalized analytical curve for the GQDs-TU photoluminescence quenching in presence of Hg^{2+} usin FIA: $y = 0.002$ (L μg^{-1}) $x + 1.0$ ($R^2 = 0.999$).

Table 8 - Figures of merit for Hg^{2+} detection using FIA.

Parameter	Value
Linear range (μgL^{-1})	100 to 900
R^2	0.999
LOD (μgL^{-1})	23.8
LOQ (μgL^{-1})	79.6
Equation of curve	$y = 0.002x + 1.0$

4.4.3
Attempts to determine Hg^{2+} using the GQDs-TU probe in flow regime

The attempts in using the GQDs-TU probe to determine Hg^{2+} were made in regime flow rather that batch analysis. Regime flow provides larger analytical frequency (estimated for the proposed method in 20 samples h^{-1}) and it is less labor-intensive.

The first sample tested was the standard solution from NIST named Mercury in Water (NIST-SRM 1641c) which indicates, as a reference value, 1.47 ± 0.04 mg L^{-1} of Hg^{2+}. Sample was diluted with ultrapure water in order to adjust concentration (to 375 μg L^{-1}) within the range of the proposed

method. The results obtained for the SRM was significantly higher, with a stronger quenching effect than expected, which resulted in a value out of the analytical range of the curve (> 900 μg L^{-1}). Such result indicated two possibilities: interferences imposed by sample matrix or a problem with the SRM as the available sample, presented in a sealed ampoule, was more than 10 years old and therefore with expired date for the reference value.

Analysis of the same sample was made using cold-vapor atomic absorption spectrometry after reduction of Hg^{2+} using SnCl$_2$, and the result was 1.58 ± 0.08 mg L^{-1}, which ruled out any concern related to the quality of the SRM. Information provided by the NIST-SRM 1641c certicate of analysis indicated that high purity gold (dissolved in *aqua-regia*) was included (~1 mg kg^{-1}) into the SRM matrix in order to stabilize mercury, providing long term validity period of the material. In order to evaluate if gold would promote interference in the determination of Hg^{2+}, additions of increasing aliquots of a standard solution of gold were made into the GQDs-TU probe. As seen in Figure 31, a strong photoluminescence quenching effect was observed. Such interference may be explained by the affinity of gold ions towards sulfurated groups, affecting the ones on the surface of the GQDs-TU.
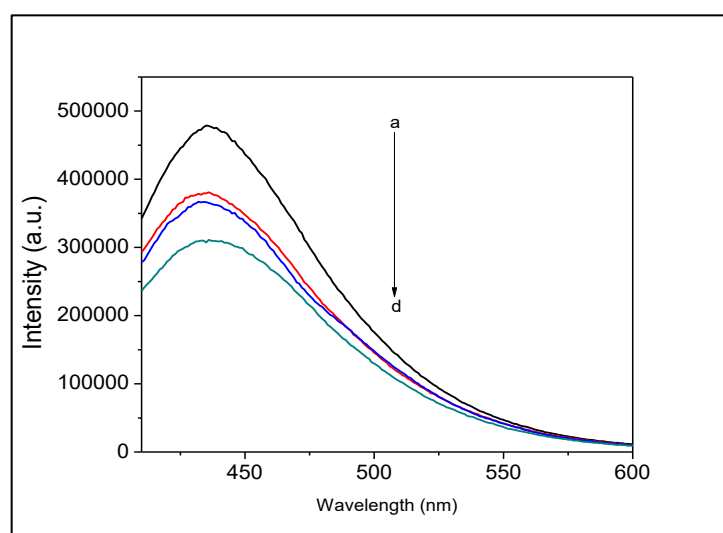
Figure 31 - Photoluminescence from the GQDs-TU dispersion in the presence of increasing concentrations of Au^{3+}: a) 0; b) 100 μg L^{-1}; c) 300 μg L^{-1}; d) 600 μg L^{-1}.

The second sample tested was a simulated mineral water with low

content of alkaline and alkaline earth ions. Sample was fortified with Hg^{2+} at 375 μg L^{-1} and with the following ions: Na^+ (6 μg L^{-1}), K^+ (10 μg L^{-1}), Ca^{2+} (10 μg L^{-1}) and Mg^{2+} (6 μg L^{-1}). This sample was analysed and percent recovery was (99.4 ± 1.2) % (n = 4). Fiagram with analytical response form standards and the signal measured for the sample is presented in Figure 32.
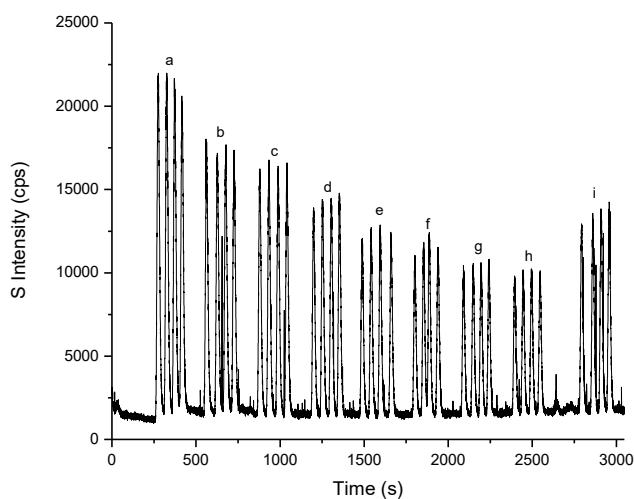
Figure 32 – Fiagram from the analysis of simulated mineral water sample. Standard solutions of Hg^{2+} at a) 0; b) 100; c) 150; d) 300; e) 450; f) 600; g) 750; h) 900 µg L^{-1} and i) sample (375 µg L^{-1} of Hg^{2+}).

5
Conclusions

The feasibility of a turn-off photoluminescent probe for detection of Hg^{2+} was evaluated and further extended to the practical flow injection assay in synthetic samples. Four kinds of graphene quantum dots were synthesized aiming to find the adequate one to be used as photoluminescent probe. The nanoparticles evaluated as the best "turn-off" photoluminescent probe was the one functionalized with thiourea (GQDs-TU) due to fast interaction with analyte, stability and intensity variation of the response. The variation in response towards Hg^{2+} indicate that produced GQDs are different in terms of chemical groups present onto nanoparticle surface and edges. Behavior of the system under different temperatures and the ξ-potentials indicated that a complex species (indicated as GQDs-TU-Hg^{2+}) is formed, not necessarily with a defined stoichiometry, resulting in the signal quenching.

Batch assay was carried out by measuring the photoluminescence from the probe dispersion after the addition of different concentration of Hg^{2+} produced a linear trend in quenching (normalized photoluminescence values) with LOQ of 10 μg L^{-1}. Under flow regime, LOQ decreased to about 80 μg L^{-1} but allowed high analytical frequency. Studies have demonstrated that matrix components present in natural waters produces severe interferences that would be only minimized if they are present at low concentrations or if Hg^{2+} is somehow separated from sample before analysis. Neither chelation nor matrix matching was efficient in eliminating such problem. For a controlled and simulated sample, though, percent recovery was 99.4 ± 1.2 % (n = 4).

Not only were the GQDs-TU practical and straightforward to synthesize, this probe is probably less toxic than the ones made of semiconductor QDs containing Cd. It is also worth to mention that the use of FIA in assays using GQDs has not been properly explored in the literature and this work has accessed the behavior of these nanoparticles systems in

terms of reproducibility of interaction with analyte, dispersion of sample zone and resolution in response during an assay.

6
Future work

Important points may still be addressed to complement this work. In terms of the nanoparticles production, a systematic study concerning preparation of GQDs-TU must be made in order to make clear which parameters, related to the hydro-exfoliation procedure, are the most critical in producing uniform batches of nanoparticles. More studies (characterizations) are also required to understand differences in functionalizations produced onto nanoparticles when using different chemical substances as starting materials.

In terms of the method, procedures to separate Hg^{2+} from matrix must be studied and the most promising one is the distillation of sample, in an excess of chloride to produce $Hg(Cl)_n^{(2-n)+}$ species, transferring mercury along the distillated fraction. Finding a proper pre-concentration procedure may also improve the sample limit of detection and the viability of the method to access water samples with less concentrations of Hg^{2+}.

The method may also be adapted to determine thiomersal after applying a photo-degradation that quantitatively produce the detected Hg^{2+} (procedure developed by J. Miranda-Andrades *et al.* [30]) aiming the analysis of pharmaceutical samples or waste water from pharmaceutical industries.

7
References

[1]   F. Zahir, S. J. Rizwi, S. K. Haq, e R. H. Khan, "Low dose mercury toxicity and human health", *Environ. Toxicol. Pharmacol.*, vol. 20, nº 2, p. 351–360, 2005.

[2]   S. Wang *et al.*, "Branch-Migration based Fluorescent Probe for Highly Sensitive Detection of Mercury", *Anal. Chem.*, p. acs.analchem.8b03547, 2018.

[3]   B. Manna e C. R. Raj, "Nanostructured Sulfur-Doped Porous Reduced Graphene Oxide for the Ultrasensitive Electrochemical Detection and Efficient Removal of Hg(II)", *ACS Sustain. Chem. Eng.*, vol. 6, nº 5, p. 6175–6182, 2018.

[4]   K. Srinivasan, K. Subramanian, K. Murugan, e K. Dinakaran, "Sensitive fluorescence detection of mercury(<scp>ii</scp>) in aqueous solution by the fluorescence quenching effect of MoS $_2$ with DNA functionalized carbon dots", *Analyst*, vol. 141, nº 22, p. 6344–6352, 2016.

[5]   B. Passariello, M. Barbaro, S. Quaresima, A. Casciello, e A. Marabini, "Determination of mercury by inductively coupled plasma - Mass spectrometry", *Microchem. J.*, vol. 54, nº 4, p. 348–354, 1996.

[6]   H. Morita, H. Tanaka, e S. Shimomura, "Atomic fluorescence spectrometry of mercury: principles and developments", *Spectrochim. Acta Part B At. Spectrosc.*, vol. 50, nº 1, p. 69–84, 1995.

[7]   S. Zhu, B. Chen, M. He, e T. Huang, "Speciation of mercury in water and fish samples by HPLC-ICP-MS after magnetic solid phase extraction", *Talanta*, vol. 171, p. 213–219, 2017.

[8]   B. Jackson, V. Taylor, R. A. Baker, e E. Miller, "Low-Level Mercury Speciation in Freshwaters by Isotope Dilution GC-ICP-MS", *Environ. Sci. Technol.*, vol. 43, nº 7, p. 2463–2469, abr. 2009.

[9]   J. Murphy, P. Jones, e S. J. Hill, "Determination of total mercury in environmental and biological samples by flow injection cold vapour atomic absorption spectrometry", *Spectrochim. Acta Part B At. Spectrosc.*, vol. 51, nº 14, p. 1867–1873, dez. 1996.

[10]   D. Han *et al.*, "A regenerative electrochemical sensor based on oligonucleotide for the selective determination of mercury (II)", *Analyst*, vol. 134, nº 9, p. 1857–1862, 2009.

[11]   G. Cabello-Carramolino e M. D. P. Dominguez, "Application of new sol – gel electrochemical sensors to the determination of trace mercury", *Anal. Chim. Acta*, vol. 614, nº 1, p. 103–111, 2008.

[12]   T. Alizadeh, M. Reza, e M. Zare, "Analytica Chimica Acta Application of an Hg 2 + selective imprinted polymer as a new modifying agent for the preparation of a novel highly selective and sensitive

electrochemical sensor for the determination of ultratrace mercury ions", *Anal. Chim. Acta*, vol. 689, nº 1, p. 52–59, 2011.

[13] B. Liu, Y. Huang, X. Zhu, Y. Hao, Y. Ding, e W. Wei, "Smart lanthanide coordination polymer fl uorescence probe for mercury (II) determination", *Anal. Chim. Acta*, vol. 912, p. 139–145, 2016.

[14] H. Tan, Y. Zhang, e Y. Chen, "Sensors and Actuators B : Chemical Detection of mercury ions (Hg 2 +) in urine using a terbium chelate fluorescent probe", *Sensors Actuators B. Chem.*, vol. 156, nº 1, p. 120–125, 2011.

[15] H. Tan, B. Liu, e Y. Chen, "Lanthanide Coordination Polymer Nanoparticles for Sensing of Mercury (II) by Photoinduced Electron Transfer", *ACS Nano*, vol. 6, nº 12, p. 10505–10511, 2012.

[16] H. Wang, Y. Yang, C. Zeng, T. Chu, Y. Zhu, e S. W. Ng, "A highly luminescent terbium–organic framework for reversible detection of mercury ions in aqueous solution", *Photochem. Photobiol. Sci.*, vol. 12, p. 1700–1706, 2013.

[17] P. Wu *et al.*, "Cadmium-Based Metal − Organic Framework as a Highly Selective and Sensitive Ratiometric Luminescent Sensor for Mercury(II)", *Inorg. Chem.*, vol. 54, nº 23, p. 11046–11048, 2015.

[18] H. Li, Y. Zhang, X. Wang, e Z. Gao, "A luminescent nanosensor for Hg (II) based on functionalized CdSe / ZnS quantum dots", *Microchim Acta*, vol. 160, p. 119–123, 2008.

[19] H. Li, Y. Zhang, X. Wang, D. Xiong, e Y. Bai, "Calixarene capped quantum dots as luminescent probes for Hg 2+ ions", *Mater. Lett.*, vol. 61, p. 1474–1477, 2007.

[20] M. Koneswaran e R. Narayanaswamy, "Mercaptoacetic acid capped CdS quantum dots as fluorescence single shot probe for mercury (II)", *Sensors Actuators B Chem.*, vol. 139, p. 91–96, 2009.

[21] Y. Kim, R. C. Johnson, e J. T. Hupp, "Gold Nanoparticle-Based Sensing of 'Spectroscopically Silent' Heavy Metal Ions", *Nano Lett.*, vol. 1, nº 4, p. 165–167, 2001.

[22] B. C. Ye e B. C. Yin, "Highly sensitive detection of mercury(II) ions by fluorescence polarization enhanced by gold nanoparticles", *Angew. Chemie - Int. Ed.*, vol. 47, nº 44, p. 8386–8389, 2008.

[23] M. Li, Q. Wang, X. Shi, L. A. Hornak, e N. Wu, "Detection of mercury(II) by quantum dot/DNA/gold nanoparticle ensemble based nanosensor via nanometal surface energy transfer", *Anal. Chem.*, vol. 83, nº 18, p. 7061–7065, 2011.

[24] D. Huang, C. Niu, M. Ruan, X. Wang, G. Zeng, e C. Deng, "Highly sensitive strategy for Hg2+ detection in environmental water samples using long lifetime fluorescence quantum dots and gold nanoparticles.", *Environ. Sci. Technol.*, vol. 47, nº 9, p. 4392–8, 2013.

[25] D. XIANG, K. ZHAI, Q. SANG, B. SHI, e X. YANG, "Highly Sensitive Fluorescence Quantitative Detection of Mercury in Soil Based on Non-labeled Molecular Beacon and Fluorescent Dye Hoechst 33258",

Anal. Sci., vol. 33, nº 3, p. 275–279, 2017.

[26] Z. Lin, X. Li, e H. B. Kraatz, "Impedimetric immobilized DNA-based sensor for simultaneous detection of Pb2+, Ag+, and Hg2+", *Anal. Chem.*, vol. 83, nº 17, p. 6896–6901, 2011.

[27] M. Jia, Z. Zhang, J. Li, H. Shao, L. Chen, e X. Yang, "Sensors and Actuators B : Chemical A molecular imprinting fluorescence sensor based on quantum dots and a mesoporous structure for selective and sensitive detection of 2 , 4-dichlorophenoxyacetic acid", *Sensors Actuators B. Chem.*, vol. 252, p. 934–943, 2017.

[28] S. Suresh, "Semiconductor Nanomaterials , Methods and Applications : A Review", *Nanosci. Nanotechnol.*, vol. 3, nº 3, p. 62–74, 2013.

[29] R. Koole, E. Groeneveld, e D. Vanmaekelbergh, *Size Effects on Semiconductor Nanoparticles*. 2014.

[30] J. R. Miranda-Andrades, S. Khan, C. A. T. Toloza, E. C. Romani, F. L. Freire Júnior, e R. Q. Aucelio, "Thiomersal photo-degradation with visible light mediated by graphene quantum dots: Indirect quantification using optical multipath mercury cold-vapor absorption spectrophotometry", *Spectrochim. Acta - Part B At. Spectrosc.*, vol. 138, p. 81–89, 2017.

[31] F. Yan, Y. Zou, M. Wang, X. Mu, N. Yang, e L. Chen, "Highly photoluminescent carbon dots-based fluorescent chemosensors for sensitive and selective detection of mercury ions and application of imaging in living cells", *Sensors Actuators, B Chem.*, vol. 192, p. 488–495, 2014.

[32] C. A. T. Toloza, S. Khan, R. L. D. Silva, E. C. Romani, F. L. Freire, e R. Q. Aucélio, "Different approaches for sensing captopril based on functionalized graphene quantum dots as photoluminescent probe", *J. Lumin.*, vol. 179, p. 83–92, 2016.

[33] W. A.-J. XU Yue, TANG Chun-Jing, HUANG Hong, SUN Chao-Qun, ZHANG Ya-Kun, YE Qun-Feng, "Green Synthesis of Fluorescent Carbon Quantum Dots for Detection of Hg2+", *Chinese J. Anal. Chem.*, vol. 42, nº 9, p. 1252–1258, 2014.

[34] C. A. T. Toloza *et al.*, "Photoluminescence suppression effect caused by histamine on amino-functionalized graphene quantum dots with the mediation of Fe3 +, Cu2 +, Eu3 +: Application in the analysis of spoiled tuna fish", *Microchem. J.*, vol. 133, p. 448–459, 2017.

[35] P. B. Stockwell, "The Role of Flow Injection Analysis Within the Framework of an Automated Laboratory", *J. Automat. Chem.*, vol. 12, nº 3, p. 95–103, 1990.

[36] W. L. Clevenger, B. W. Smith, e J. D. Winefordner, "Trace Determination of Mercury : A Review", *Crit. Rev. Anal. Chem.*, vol. 27, nº 1, p. 1–26, 1997.

[37] M. Q. Zhang, Y. C. Zhu, e R. W. Deng, "Evaluation of mercury emissions to the atmosphere from coal combustion, China.", *Ambio,*

vol. 31, nº 6, p. 482–4, 2002.

[38] R. Kessler, "The Minamata convention on mercury: A first step toward protecting future generations", *Environ. Health Perspect.*, vol. 121, nº 10, p. 304–309, 2013.

[39] U. N. E. Programme, "Minamata convention on mercury. TEXT AND ANNEXES", *United Nations Environment Programme*, 2017. [Online]. Available at: http://www.mercuryconvention.org/Convention/Text. [Acessado: 17-fev-2019].

[40] IPCS, "Methylmercury", *World Heal. Organ. Geneva*, vol. 101, 1990.

[41] World Health Organisation, "Mercury in Drinking-water, Background document for development of WHO Guidelines for Drinking-water Quality", 2005.

[42] UWEC, "Mercury in the Environment and Water Supply", *University of Wisconsin Eau Claire*, 1992. [Online]. Available at: https://people.uwec.edu/piercech/Hg/mercury_water/drinkingwater.htm. [Acessed: 14-jul-2019].

[43] H. Hintelamnn, R. D. Evans, e J. Y. Villeneuve, "Measurement of Mercury Methylation in Sediments by Using Enriched Stable Mercury Isotopes Combined with Methyl mercury Determination by Gas Chromatography-Inductively Coupled Plasma Mass Spectrometry", *J. Anal. At. Spectrom.*, vol. 10, nº September, p. 619–624, 1995.

[44] H. E. L. Armstrong, W. T. Corns, P. B. Stockwell, G. O. Connor, L. Ebdon, e E. H. Evans, "Comparison of AFS and ICP-MS detection coupled with gas chromatography for the determination of methylmercury in marine samples", vol. 390, p. 245–253, 1999.

[45] N. Bloom, "Determination of volatile mercury species at the picogram level by low-temperature gas chromatography with cold-vapour atomic fluorescence detection", *Anal. Chim. Acta*, vol. 208, p. 151–161, 1988.

[46] A. Manová *et al.*, "Preconcentration of Hg in Waters for ET AAS in a Flow-Through Electrochemical Cell", *Pol. J. Environ. Stud*, vol. 21, nº 5, p. 1313–1318, 2012.

[47] A. Niazi, T. Momeni-Isfahani, e Z. Ahmari, "Spectrophotometric determination of mercury in water samples after cloud point extraction using nonionic surfactant Triton X-114", *J. Hazard. Mater.*, vol. 165, nº 1–3, p. 1200–1203, 2009.

[48] J. Chen *et al.*, "A functionalized gold nanoparticles and Rhodamine 6G based fluorescent sensor for high sensitive and selective detection of mercury (II) in environmental water samples", *Anal. Chim. Acta*, vol. 599, p. 134–142, 2007.

[49] A. Zheng, J. Chen, G. Wu, H. Wei, C. He, e X. Kai, "Optimization of a sensitive method for the ' switch-on ' determination of mercury (II) in waters using Rhodamine B capped gold nanoparticles as a fluorescence sensor", *Microchim Acta*, vol. 164, p. 17–27, 2009.

[50] C. Huang e H. Chang, "Selective Gold-Nanoparticle-Based 'Turn-On'

Fluorescent Sensors for Detection of Mercury(II) in Aqueous Solution Chih-Ching", *Anal. Chem.*, vol. 78, nº 24, p. 8332–8338, 2006.

[51] C. Zhu, Ã. L. Li, F. Fang, J. Chen, e Y. Wu, "Functional InP Nanocrystals as Novel Near-infrared Fluorescent Sensors for Mercury Ions", *Chem. Lett.*, vol. 34, nº 7, p. 898–899, 2005.

[52] J. Chen, Y. Gao, Z. Xu, G. Wu, Y. Chen, e C. Zhu, "A novel fluorescent array for mercury (II) ion in aqueous solution with functionalized cadmium selenide nanoclusters", *Anal. Chim. Acta*, vol. 577, p. 77–84, 2006.

[53] A. J. G. Zarbin, "QUÍMICA DE (NANO)MATERIAIS Aldo J. G . Zarbin", *Quim. Nova*, vol. 30, nº 6, p. 1469–1479, 2007.

[54] Y. Zhao, *Quantum Dots and Doped Nanocrystals: Synthesis, Optical Properties and Bio-applications*, nº January. 2013.

[55] C. J. Murphy, "Optical Sensing with Quantum Dots", *Anal. Chem.*, vol. 91, p. 520A–526A, 2002.

[56] J. Machado de Carvalho, K. C. Leandro, e R. Q. Aucélio, "Estudo do comportamento dos quantum dots em meio aquoso e aplicação destes nanomateriais como sonda para determinação de rutina e quercetina", Pontifícia Universidade Católica do Rio de Janeiro., 2014.

[57] Y. Xu, N. Al-Salim, C. W. Bumby, e R. D. Tilley, "Synthesis of SnS Quantum Dots Experimental Section", *Am. Chem. Soc.*, nº 131, p. 15990–15991, 2009.

[58] R. De Angelis *et al.*, "Chemical Sensitivity of Luminescent Epitaxial Surface InP Quantum Dots", vol. 2013, nº March, p. 1–5, 2013.

[59] L. Brus, "Electronic wave functions in semiconductor clusters: Experiment and theory", *J. Phys. Chem.*, vol. 90, nº 12, p. 2555–2560, 1986.

[60] S. V. Gaponenko, "Optical Properties of Semiconductor Nanocrystals", vol. 157, p. 260, 2005.

[61] T. Torchynska e Y. Vorobiev, "Semiconductor II-VI Quantum Dots with Interface States and Their Biomedical Applications", *Adv. Biomed. Eng.*, 2011.

[62] R. E. Galian e M. de la Guardia, "The use of quantum dots in organic chemistry", *TrAC - Trends Anal. Chem.*, vol. 28, nº 3, p. 279–291, 2009.

[63] F. H. Quina, "Nanotecnologia e o meio ambiente: Perspectivas e riscos", *Quim. Nova*, vol. 27, nº 6, p. 1028–1029, 2004.

[64] A. Devrim, G. Pawel Potasz, M. Korkusinski, e P. Hawrylak, *NanoScience and Technology - Graphene Quantum Dots*. Springer, 2014.

[65] Z. Zhang, J. Zhang, N. Chen, e L. Qu, "Graphene quantum dots: An emerging material for energy-related applications and beyond", *Energy Environ. Sci.*, vol. 5, nº 10, p. 8869–8890, 2012.

[66] J. Shen, Y. Zhu, X. Yang, e C. Li, "Graphene quantum dots: emergent nanolights for bioimaging, sensors, catalysis and photovoltaic devices Jianhua", *ChemComm*, vol. 48, p. 3686–3699, 2012.

[67] L. Wang, H. Li, T. Tu, G. Cao, e C. Zhou, "Controllable tunnel coupling and molecular states in a graphene double quantum dot Controllable tunnel coupling and molecular states in a graphene double quantum dot", *Appl. Phys. Lett.*, vol. 100, n° 022106, p. 022106/1-022106/5, 2012.

[68] M. Zhang *et al.*, "Facile synthesis of water-soluble , highly fluorescent graphene quantum dots as a robust biological label for stem cells", *J. Mater. Chem.*, vol. 22, n° 15, p. 7461–7467, 2012.

[69] S. Zhuo, M. Shao, e S. Lee, "Upconversion and Downconversion Fluorescent Graphene Quantum Dots : Ultrasonic Preparation and", *ACS Nano*, vol. 6, n° 2, p. 1059–1064, 2012.

[70] S. Zhu *et al.*, "Graphene quantum dots with controllable surface oxidation, tunable fluorescence and up-conversion emission", *RSC Adv.*, vol. 2, n° 7, p. 2717–2720, 2012.

[71] D. Pan, J. Zhang, Z. Li, e M. Wu, "Hydrothermal route for cutting graphene sheets into blue-luminescent graphene quantum dots", *Adv. Mater.*, vol. 22, n° 6, p. 734–738, 2010.

[72] N. Mohanty *et al.*, "and dispersible graphene nanostructures of controlled shape and size", *Nat. Commun.*, vol. 3, n° May, p. 844–848, 2012.

[73] L. Tang *et al.*, "Deep Ultraviolet Photoluminescence of Water-Soluble Self-Passivated Graphene Quantum Dots", *ACS Nano*, vol. 6, n° 6, p. 5102–5110, 2012.

[74] K. Habiba, V. I. Makarov, Brad R. Weiner and, e Gerardo Morell, "Fabrication of Nanomaterials by Pulsed Laser Synthesis", in *Manufacturing Nanostructures (OCN)*, n° September, A. Waqar e A. N, Orgs. UK: Once Central Press (OCN), 2014, p. 263–292.

[75] J. Wang *et al.*, "Opportunities and Challenges of Fluorescent Carbon Dots in Translational Optical Imaging", *Curr. Pharm. Des.*, vol. 21, n° 00, 2015.

[76] J. Peng, J. Guan, L.-P. Jiang, e J.-J. Zhu, "Biological Application of Luminescent Graphene Quantum Dots", *Sci. Adv. Mater.*, vol. 7, n° 10, p. 1945–1961, 2015.

[77] J. J. Liu, X. L. Zhang, Z. X. Cong, Z. T. Chen, H. H. Yang, e G. N. Chen, "Glutathione-functionalized graphene quantum dots as selective fluorescent probes for phosphate-containing metabolites", *Nanoscale*, vol. 5, n° 5, p. 1810–1815, 2013.

[78] V. Georgakilas *et al.*, "Functionalization of graphene: Covalent and non-covalent approach", *Chem. Rev.*, vol. 112, n° 11, p. 6156–6214, 2012.

[79] H. Sun, N. Gao, L. Wu, J. Ren, W. Wei, e X. Qu, "Highly photoluminescent amino-functionalized graphene quantum dots used

for sensing copper ions", *Chem. - A Eur. J.*, vol. 19, nº 40, p. 13362–13368, 2013.

[80] Y. Li *et al.*, "An electrochemical avenue to green-luminescent graphene quantum dots as potential electron-acceptors for photovoltaics", *Adv. Mater.*, vol. 23, nº 6, p. 776–780, 2011.

[81] Y. Li *et al.*, "Nitrogen-doped graphene quantum dots with oxygen-rich functional groups", *J. Am. Chem. Soc.*, vol. 134, p. 15–18, 2012.

[82] A. Ananthanarayanan *et al.*, "Nitrogen and phosphorus co-doped graphene quantum dots: Synthesis from adenosine triphosphate, optical properties, and cellular imaging", *Nanoscale*, vol. 7, nº 17, p. 8159–8165, 2015.

[83] J. Shen, Y. Zhu, X. Yang, J. Zong, J. Zhang, e C. Li, "One-pot hydrothermal synthesis of graphene quantum dots surface-passivated by polyethylene glycol and their photoelectric conversion under near-infrared light", *New J. Chem.*, vol. 36, nº 1, p. 97–101, 2012.

[84] M. Shamsipur, A. Barati, e S. Karami, "Long-wavelength, multicolor, and white-light emitting carbon-based dots: Achievements made, challenges remaining, and applications", *Carbon N. Y.*, vol. 124, p. 429–472, 2017.

[85] G. Eda *et al.*, "Blue photoluminescence from chemically derived graphene oxide", *Adv. Mater.*, vol. 22, nº 4, p. 505–509, 2010.

[86] D. Pan, J. Zhang, Z. Li, C. Wu, e M. Wu, "Observation of pH-, solvent-, spin-, and excitation-dependent blue photoluminescence from carbon nanoparticles", *Chem. Commun.*, vol. 46, p. 3681–3683, 2010.

[87] J. Wang e Z. Li, "N-Doped Graphene Quantum Dots via Thermal Pyrolysis of Fumaric Acid for Optical Detection of Hg2+", *Synth. Catal.*, vol. 2, nº 1, p. 1–4, 2017.

[88] Y. Yang *et al.*, "The Fluorescent Quenching Mechanism of N and S Co-Doped Graphene Quantum Dots with Fe 3 + and Hg 2 + Ions and Their Application as a Novel Fluorescent Sensor", *Nanomaterials*, vol. 9, nº 738, p. 1–17, 2019.

[89] J. Li, B. Du, Y. Li, Y. Wang, D. Wu, e Q. Wei, "A turn-on fluorescent sensor for highly sensitive mercury(<scp>ii</scp>) detection based on a carbon dot-labeled oligodeoxyribonucleotide and MnO 2 nanosheets", *New J. Chem.*, vol. 42, nº 2, p. 1228–1234, 2018.

[90] R. Beicher *et al.*, "RECOMMENDED NOMENCLATURE FOR AUTOMATIC ANALYSIS", London, 1970.

[91] T. Kikas, "Introduction to Flow Injection Analysis (FIA) - Determination of Chloride Ion Concentration", *chemistry.gatech.edu*. [Online]. Available at: ww2.chemistry.gatech.edu/class/analyt/fia.pdf. [Acessado: 09-fev-2019].

[92] A. M. Brouwer, "Standards for photoluminescence quantum yield measurements in solution (IUPAC Technical Report)*", *Pure Appl.*

Chem, vol. 83, nº 12, p. 2213–2228, 2011.

[93] S. L. Walker, S. Bhattacharjee, E. M. V Hoek, e M. Elimetech, "A Novel Asymmetric Clamping Cell for Measuring Streaming Potential of Flat Surfaces", *Langmuir*, vol. 18, p. 2193–2198, 2002.

[94] T. A. Schoenmakers TJ, Visser GJ, Flik G, "CHELATOR: An Improved Method for Computing Metal Ion Concentrations in Physiological Solutions.", *Biotechniques*, vol. 12, p. 870–879, 1992.

[95] M. Thompson e S. L. R. Ellison, "A review of interference effects and their correction in chemical analysis with special reference to uncertainty", *Accredit. Qual. Assur.*, vol. 10, nº 3, p. 82–97, 2005.

[96] C. C. Painton e H. A. Mottola, "Kinetics in continuous flow sample processing Chemical Contributions to Dispersion in Flow-Injection Techniques", *Anal. Chim. Acta*, vol. 158, nº C, p. 67–84, 1984.

8
Supplementary material

A

Table S1 – List of commercial mineral water with chemical composition

	Chemical composition (mg L^{-1})				
	Brand				
	Da Montanha	**Petropolis**	**Sao Lourenco**	**Nestle**	**L'Aqua**
Bicarbonate	45.600	7.270	286.730	13.300	24.970
Calcium	10.450	2.690	28.169	1.711	2.652
Sodium	9.190	1.904	36.040	3.350	5.047
Potassium	2.008	0.960	31.346	0.961	0.750
Fluoride	0.120	-	0.150	0.020	0.020
Magnesium	1.537	0.450	12.491	0.500	1.459
Nitrate	3.680	4.540	1.500	1.110	0.28
Chloride	7.190	2.260	1.610	1.730	2.300
Sulfate	4.100	1.120	2.170	0.800	0.620
Strontium	0.124	0.014	0.053	0.015	0.028
Barium	0.065	0.018	0.408	0.019	0.042
pH @25ºC	6.13	5.86	5.25	5.61	5.71